bioRxiv preprint doi: https://doi.org/10.1101/2020.10.11.335448; this version posted October 11, 2020. The copyright holder for this preprint (which was not certified by peer review) is the author/funder. All rights reserved. No reuse allowed without permission.

Title

TWIST1 controls cellular senescence and energy metabolism in mesenchymal stem cells

Author names and affiliations

Chantal Voskamp[1], Laura A. Anderson[1], Wendy J. L. M. Koevoet[2], Sander Barnhoorn[3], Pier G. Mastroberardino[3], Gerjo J.V.M. van Osch[1,2], Roberto Narcisi[1]

1 Department of Orthopaedics, Erasmus MC, University Medical Center, 3015 CN Rotterdam, the Netherlands

2 Department of Otorhinolaryngology, Erasmus MC, University Medical Center, 3015 CN Rotterdam, the Netherlands

3 Departments of Molecular Genetics, Erasmus MC, University Medical Center, 3015 CN Rotterdam, the Netherlands

Contact corresponding author

Roberto Narcisi

Department of Orthopaedics, Erasmus MC, 3015 CN Rotterdam, the Netherlands

Email: r.narcisi@erasmusmc.nl

Tel.: +31-10-7044626

bioRxiv preprint doi: https://doi.org/10.1101/2020.10.11.335448; this version posted October 11, 2020. The copyright holder for this preprint (which was not certified by peer review) is the author/funder. All rights reserved. No reuse allowed without permission.

Abstract

Mesenchymal stem cells (MSC) are promising cells for regenerative medicine therapies, because they can differentiate towards multiple cell lineages. However, heterogeneity in differentiation capacity is one of the main drawbacks that limit their use clinically. Differences in the occurrence of cellular senescence and in the expression of the senescence associated secretory phenotype (SASP) in MSC populations contribute to their heterogeneity. Here, we show the involvement of *TWIST1* expression in the regulation of MSC senescence, demonstrating that silencing of *TWIST1* in MSCs increased the occurrence of senescence. These senescent MSCs had a SASP that was different from irradiation-induced senescent MSCs. In addition, metabolic evaluation performed by the Seahorse XF apparatus showed that both *TWIST1* silencing-induced and irradiation-induced senescent MSCs had a higher oxygen consumption compared to control MSCs, while *TWIST1* silencing-induced senescent MSCs had a low extracellular acidification rate compared to the irradiation-induced senescent MSCs. Overall, our data indicate how *TWIST1* regulation influences senescence in human MSCs and that *TWIST1* silencing-induced senescence is characterized by a specific expression of the SASP and the metabolic state.

Keywords: TWIST1, mesenchymal stem cells, cellular senescence, SASP, metabolism

bioRxiv preprint doi: https://doi.org/10.1101/2020.10.11.335448; this version posted October 11, 2020. The copyright holder for this preprint (which was not certified by peer review) is the author/funder. All rights reserved. No reuse allowed without permission.

Introduction

Regenerative medicine strategies aim to regenerate tissues that have been damaged by injury or pathology. A promising cell source for regenerative medicine therapies is the multipotent progenitor cell referred to as mesenchymal stem cell (MSC). MSCs have the capacity to self-renew, and to differentiate towards multiple lineages (Pittenger et al., 1999). MSCs can be isolated from several tissues such as the bone marrow (Haynesworth et al., 1992; Pittenger et al., 1999), umbilical cord blood (Erices et al., 2000; Romanov et al., 2003), or adipose tissue (Halvorsen et al., 2000; Zuk et al., 2001). However, a limitation that hinders the clinical use of MSCs is their inter- and intra- donor variation in differentiation capacity. This heterogeneity includes the occurrence of cellular senescence (Li et al., 2017). Cellular senescence is an irreversible state in which cells undergo permanent cell cycle arrest, while the cells are still metabolically active and can secrete pro-inflammatory factors. These secreted factors are named the senescence-associated secretory phenotype (SASP) (Lunyak et al., 2017). The occurrence of the SASP is linked to the metabolic state of the cell (Dörr et al., 2013; Wiley et al., 2016). Glycolysis, which breaks down glucose into pyruvate, ATP and NADH, has been demonstrated to be increased in senescent cells (Bittles and Harper, 1984; James et al., 2015). In addition, senescent fibroblasts can have an impaired mitochondrial metabolism (Wiley et al., 2016).

Cellular senescence has been shown to reduce the differentiation capacity of umbilical cord-derived MSCs (Cheng et al., 2011) and could also be unsafe for regenerative medicine strategies, since senescent MSCs can promote tumor formation (Hochane et al., 2017; Li et al., 2015). In addition senescent cells transplanted in the knee joint of mice can induce an osteoarthritis-like phenotype showing reduced cartilage content, osteophyte formation and subchondral bone structure alterations (Xu et al., 2017). Safe and reproducible clinical use of MSCs requires a better understanding of the molecular mechanisms behind cellular senescence and their SASP profile.

Previously, we and others observed that MSC expansion was associated with the expression of the transcription factor *TWIST1* (Isenmann et al., 2009; Narcisi et al., 2015; Voskamp et al., 2020).

bioRxiv preprint doi: https://doi.org/10.1101/2020.10.11.335448; this version posted October 11, 2020. The copyright holder for this preprint (which was not certified by peer review) is the author/funder. All rights reserved. No reuse allowed without permission.

Moreover, TWIST1 can regulate the expression of cellular senescence marker P21 in hypoxic MSC cultures (Tsai et al., 2011). To better understand the molecular mechanism behind cellular senescence in MSCs, we investigated how *TWIST1* expression regulates cellular senescence and their SASP expression. In this study we show that *TWIST1* overexpression in MSCs inhibited cellular senescence, while silencing of *TWIST1* induced cellular senescence. In addition, we show that *TWIST1* can modulate the SASP and bioenergetic profile in senescent MSCs. These results provide novel molecular insights in SASP and metabolism regulation and suggest that TWIST1 could be a target to modulate cellular senescence.

Results and Discussion

TWIST1 expression is negatively associated with cellular senescence in MSCs

To determine whether *TWIST1* expression is involved in cellular senescence in human MSCs, we started by analyzing its expression in senescent MSCs. Cellular senescence was induced in MSCs by gamma irradiation (20 Gy) and confirmed by SA-β-gal staining (**Figure 1A**). *TWIST1* expression was significantly reduced in irradiated-induced senescent MSCs compared to mock irradiated MSCs (**Figure 1B**; p=0.022), indicating that *TWIST1* expression is negatively associated with cellular senescence in MSCs. Following this observation, we hypothesized that high expression of *TWIST1* is able to delay the entrance into the senescence state during passaging *in vitro*. To test this hypothesis, *TWIST1* was overexpressed in MSCs by a lentiviral-based approach. Transduction was determined by the percentage of GFP positive cells (>65% transduced cells; **Fig EV1**) and overexpression confirmed by qPCR analysis (103-fold increase compared to empty vector control; **Figure 1C**). Control and *TWIST1* overexpressing MSCs were then serially passaged for 11 days, followed by SA-β-gal analysis (**Fig EV2**). *TWIST1* overexpressing MSCs showed 15% SA-β-gal low positive cells and 0.4% SA-β-gal high positive cells, while empty vector control cells had 52% SA-β-gal low positive cells (p<0.001) and

bioRxiv preprint doi: https://doi.org/10.1101/2020.10.11.335448; this version posted October 11, 2020. The copyright holder for this preprint (which was not certified by peer review) is the author/funder. All rights reserved. No reuse allowed without permission.

2% high positive cells (p=0.052; **Figure 1D**). These results suggest that *TWIST1* expression can inhibit cellular senescence in MSC.

It has been reported that *TWIST1* expression suppresses senescence in lung and breast cancer cells (Burns et al., 2013; Nayak et al., 2017; Tran et al., 2012). In MSCs, a high *TWIST1* expression has been associated with rapid cell growth and a high proliferation capacity of MSCs (Boregowda et al., 2016; Isenmann et al., 2009; Voskamp et al., 2020). Our data indicate a direct link between *TWIST1* expression and cellular senescence in MSCs.

TWIST1 silencing induces cellular senescence with a specific senescence associated secretory phenotype in MSCs.

To elucidate whether cellular senescence can be induced via *TWIST1* modulation, *TWIST1* expression was silenced in MSCs using a siRNA approach. After 24 h of *TWIST1* siRNA treatment (siTWIST1-MSCs) *TWIST1* mRNA levels were 53% reduced (p=0.035) compared to scramble controls (**Fig EV3A**) and after 4 passages siTWIST1-MSCs showed 64% knockdown of *TWIST1* mRNA levels (p<0.001; **Fig 2A**). After 4 passages, *TWIST1* silencing increased the expression of cell cycle inhibitors and senescence markers *P16* (6.5-fold, p<0.001) and *P21* (2.1-fold, p=0.060; **Fig 2B**). The expression of *P16* was already induced after 24 h of *TWIST1* silencing (1.8-fold; p=0.015; **Fig EV3B**). No differences in *P21* expression were observed after 24 h of *TWIST1* silencing (**Fig EV3C**). In addition, after 4 passages, *TWIST1* silencing increased SA-β-gal activity in MSCs (**Fig 2C and Fig EV2E**) and decreased cell expansion (**Fig 2D**), overall indicating that *TWIST1* knockdown induces senescence growth arrest. Since the SASP can drive chronic inflammation and thereby contribute to age-related diseases such as osteoarthritis and cancer (reviewed in: Loeser et al., 2016; Zhu et al., 2014), we determined the expression of the SASP-related genes *IL6*, *IL10, IL1B*, *MMP3, IL8, CCL2* and *VEGFA* in siTWiST1-MSCs. siTWIST1-MSCs expressed higher levels of *CCL2* and *IL1B* compared to control condition (3.3-fold p=0.008, 7.4-fold p=0.008, respectively; **Fig 2E**). Interestingly, the expression of *IL6, IL10, MMP3* and

bioRxiv preprint doi: https://doi.org/10.1101/2020.10.11.335448; this version posted October 11, 2020. The copyright holder for this preprint (which was not certified by peer review) is the author/funder. All rights reserved. No reuse allowed without permission.

VEGFA were not significantly affected by *TWIST1* silencing, and *IL8* was even significantly decreased (p=0.291, p=0.077, p=0.087, p=0.912, p<0.001, respectively; **Fig 2E**). These results indicate that senescence was induced in MSCs by *TWIST1* knockdown, but generating a 'non-classical' SASP profile.

The mechanism by which the SASP related genes are regulated in senescent cells is not fully understood. It is, however, known that mitochondria can induce SASP expression via increased reactive oxygen species (ROS) and JNK activation (Vizioli et al., 2020). Interestingly, cellular senescence with a different SASP profile has previously been reported in mitochondrial dysfunctional senescence (MiDAS) (Wiley et al., 2016). Cells with MiDAS appeared to have a SASP expression profile similar to siTWIST1-MSCs: they did not express *IL-6* and *IL8* and had an increased expression of *IL-10* (Wiley et al., 2016). In addition, *TWIST1* downregulation was demonstrated to promote mitochondrial dysfunction in lung cancer cells (Seo et al., 2014) and adipocytes (Lu et al., 2018). Overall, these data suggest that *TWIST1* silencing might induce cellular senescence in MSCs via mitochondrial dysfunction.

***TWIST1* silencing alters MSC bioenergetics**

To study if *TWIST1* silencing-induced senescence is induced via mitochondrial dysfunction, we determined the bioenergetic profile in siTWIST1-MSCs using a Seahorse XF-24 Extracellular Flux Analyzer. We measured the oxygen consumption rate (OCR) reflecting cellular respiration followed by subsequent measurement after injection of mitochondrial toxins: oligomycin, FCCP and antimycin A (see materials and methods and **Fig EV4A**). We first identified the optimal cell density (30,000 cells/well; **Fig EV4B**) and the ideal concentration of FCCP (2.0 μM**; Fig EV4C**) to detect OCR in human MSCs. Then, we observed a significant increase in basal respiration levels in siTWIST1-MSCs compared to scramble controls (p=0.011; **Fig 3A-C**). In addition, siTWIST1-MSCs showed a higher maximum OCR, proton leak, Adenosine Tri-Phosphate (ATP) production and spare respiratory

bioRxiv preprint doi: https://doi.org/10.1101/2020.10.11.335448; this version posted October 11, 2020. The copyright holder for this preprint (which was not certified by peer review) is the author/funder. All rights reserved. No reuse allowed without permission.

capacity compared to scramble control cells (p=0.001, p=0.006, p=0.002, p=0.002; **Fig 3D-G**). No differences in non-mitochondrial respiration were observed between scramble control cells and siTWIST1-MSCs (p=0.251; **Fig 3H**). These data indicate that that *TWIST1* silencing induces changes in the mitochondrial function in MSCs. To determine if an increased mitochondrial respiration is specific for *TWIST1* silencing-induced senescent MSCs or whether it is common for senescent MSCs, we determined the OCR in irradiated induced senescent MSCs. Similar to *TWIST1* silencing-induced senescent MSCs, irradiation-induced senescent MSCs showed higher basal OCR, maximum OCR, proton leak, ATP production and spare respiratory capacity compared to non-irradiated control cells (p<0.001, p=0.050, p=0.019, p<0.001, p=0.032; **Fig EV5A-F**), and no differences in non-mitochondrial respiration (p=0.256; **Fig EV5G**). These data suggest that both *TWIST1* silencing-induced and irradiation-induced senescent MSCs have an increased OCR. Previously, cellular senescence has been associated with an increased OCR in fetal lung cells (Quijano et al., 2012). The increased OCR in senescent MSCs can be due to an increase in mitochondrial respiration or to an increase in mitochondrial mass. An increase in mitochondrial mass in senescent cells has been reported before in fibroblasts (Correia-Melo et al., 2016; Lee et al., 2002) and can increase the levels of mitochondrial-derived reactive oxygen species (ROS) which can cause an increase in proton leak (Brookes, 2005). In both *TWIST1* silencing-induced and irradiation-induced senescent MSCs we indeed observed an increased proton leak (**Fig 3** and **Fig EV5**), suggesting that the senescent MSCs have dysfunctional mitochondria. Dysfunctional mitochondria can trigger cellular senescence (Wiley et al., 2016), and removal of mitochondria in senescent cells has been shown to reduce the senescence phenotype (Correia-Melo et al., 2016), indicating that mitochondria can induce cellular senescence, but also play a key role in the maintenance of the senescence phenotype. Despite the difference in the SASP phenotype, both *TWIST1* silencing-induced and irradiation-induced senescent MSCs showed an increased mitochondrial respiration.

bioRxiv preprint doi: https://doi.org/10.1101/2020.10.11.335448; this version posted October 11, 2020. The copyright holder for this preprint (which was not certified by peer review) is the author/funder. All rights reserved. No reuse allowed without permission.

166 In addition to mitochondrial respiration, glycolysis plays an important role in MSC energy metabolism
167 (Pattappa et al., 2011). Cellular senescence has been associated with an increased glycolytic capacity
168 after *in vitro* expansion (Bittles and Harper, 1984). As a measure of glycolytic flux in siTWIST1-MSCs,
169 we analyzed the extracellular acidification rate (ECAR). No significant differences in ECAR were
170 observed between scramble control cells and siTWIST1-MSCs (**Fig 4A-C**), indicating that *TWIST1*
171 silencing does not alter the glycolytic flux in MSCs. Irradiated MSCs had higher ECAR compared to
172 control MSCs (**Fig EV6**), confirming earlier published data in fibroblasts (James et al., 2015). These
173 data suggest that the glycolytic capacity is unaltered in siTWIST1-MSCs, in contrast to irradiation
174 induced senescent MSCs. Overall, these data show that depending on the inducer of cellular
175 senescence in MSCs, senescent MSCs can have a different bioenergetic profile.

176 In summary our study provides novel insights in the function of *TWIST1* in the regulation of cellular
177 senescence in MSCs. Furthermore, the phenotype of these senescent cells differs from irradiation-
178 induced senescent cells in the expression of the SASP expression and the bioenergetics (**Fig. 5**),
179 highlighting that senescent MSCs can be heterogeneous. Besides, our results suggest that reduction
180 of *TWIST1* expression might drive aging phenotypes of MSCs.

181

bioRxiv preprint doi: https://doi.org/10.1101/2020.10.11.335448; this version posted October 11, 2020. The copyright holder for this preprint (which was not certified by peer review) is the author/funder. All rights reserved. No reuse allowed without permission.

Materials and Methods

Cell culture

Mesenchymal stem cells (MSC), were isolated as previously described (Knuth et al., 2018) from leftover iliac crest bone chip material obtained from patients undergoing cleft palate reconstructive surgery (MEC-2014-16; 9-13 years old). MSCs were expanded in αMEM medium (Gibco, Paisley, UK) containing 10% fetal calf serum (Gibco, selected batch 41Q2047K), 1.5 µg/mL fungizone (Invitrogen, California), and 50 µg/mL gentamicin (Gibco, Carlsbad, California), 0.1 mM Ascorbic acid (Sigma-Aldrich) and 1 ng/mL FGF2 (Instruchemie, Delftzijl, The Netherlands). MSCs were cultured at a density of 2,300 cells/cm^2 at 37°C and 5% CO_2. Cells were trypsinized and refreshed twice a week. Depending on the assay and the experimental plan, passage-3 (P3) to passage-7 (P7) cells have been used.

TWIST1 silencing

To study whether silencing of *TWIST1* induced cellular senescence, MSCs in a low passage (P3-P4) were used for this experiment. MSCs were seeded at a density of 2,300 cells/cm^2 and cultured for 24 h in standard expansion medium. Next, the cells were treated with 15 nM TWIST1 (4390824, Ambion) or scramble (4390843, Ambion) siRNA in combination with Lipofectamine RNAMAX Transfection Reagent (1:1150; Invitrogen) and optiMEM (1:6; Gibco) or were left untreated. The treatment was repeated every 3-4 days for 13-14 days.

Lentiviral constructs and virus generation

To study the effect of *TWIST1* overexpression on MSC senescence, lentiviral constructs of tetracycline-inducible expression of TWIST1 and green fluorescent protein (GFP) were used. TWIST1 cDNA was cloned into a lentiviral construct under the control of the tetracycline operator. The GFP lentiviral vector was a gift from Marius Wernig's laboratory (Stanford School of Medicine, CA;

bioRxiv preprint doi: https://doi.org/10.1101/2020.10.11.335448; this version posted October 11, 2020. The copyright holder for this preprint (which was not certified by peer review) is the author/funder. All rights reserved. No reuse allowed without permission.

Addgene plasmid # 30130). An empty lentiviral construct was used as control. Third generation lentiviral particles with a VSV-G coat were generated in HEK293T cells. HEK293T cells were cultured in DMEM HG glutamax (Life Technologies, Paisley, UK) containing 10% fetal calf serum, 1 mM sodium pyruvate (Life Technologies, Paisley, UK) and non-essential amino acids (1:100; Life Technologies, Grand Island, USA) and seeded at Poly-L-Ornithine coated plates at a density of 5 x 10^6 cells per 10 cmØ dish. After 24 h cells were transfected with lentiviral packaging vectors PMDL (5 µg per 10 cmØ dish), RSV (2.5 µg per 10cmØ dish) VSV- (2.5 µg per 10 cmØ dish) and one of the experimental inserts; rtTA, TWIST1, GFP or an empty vector (10 µg per 10 cmØ dish) using polyethylenimine (1:166). Medium was refreshed 6 h post-transfection. Viral supernatants were filtered through a 0.45 µm filter 24 h following the last medium refreshment and stored at -80°C until use.

Lentiviral transduction

To study whether *TWIST1* overexpression inhibited cellular senescence, MSCs in a high passage (P7) were used for this experiment. The transduction efficiency was determined in MSCs by titration of the GFP lentivirus construct using different virus concentrations, 1:1:1, 1:1:3 and 1:1:8 (GFP: rtTA: MSC expansion medium). After transduction of the cells for 16 h, cells were washed with PBS and fresh expansion medium was added with 2 µg/ml doxycycline (Sigma Aldrich). The transduction efficiency was assessed by analysis of the percentage of GFP positive cells using fluorescent microscopy and flow cytometry. For flow cytometry analysis, GFP transduced MSCs were fixed in 2% formaldehyde (Fluka) and filtered through 70-µM filters. Untransduced MSCs were used as a negative control. Samples were analyzed by flow cytometry using a BD Fortessa machine (BD Biosciences). The data were analyzed using FlowJo V10 software. Both fluorescent microscopy and flow cytometry showed that 65% of the cells were positive for GFP using a concentration of 1:1:1 lentivirus (**Fig EV1**), indicating that the MSCs were effectively transduced.

mRNA analysis

bioRxiv preprint doi: https://doi.org/10.1101/2020.10.11.335448; this version posted October 11, 2020. The copyright holder for this preprint (which was not certified by peer review) is the author/funder. All rights reserved. No reuse allowed without permission.

For each experiment involving RNA evaluation, the medium was renewed 24 h before harvesting the cells. MSCs were washed with PBS and lysed in RLT with 1% β-mercaptoethanol, subsequently RNA was isolated from the cells using the RNeasy micro kit (Qiagen, Hilden, Germany) according to manufactures' instructions. cDNA was synthesized using the RevertAid First-Strand cDNA Synthesis Kit (Thermo Fisher Scientific, Vilnius, Lithuania). Real-time polymerase chain reactions were performed with TaqMan Universal PCR MasterMix (Applied Biosystems) or SYBR Green MasterMix (Fermentas) using a CFX96TM PCR detection system (Bio-Rad). Primers are listed in **Table EV1** and housekeeping genes *GAPDH*, *HPRT1* and *RPS27A* were chosen for their stability in MSCs and the best housekeeping index (BHI) was calculated according to the $(Ct^{GAPDH} * Ct^{HPRT} * Ct^{RPS27A})^{1/3}$ formula. The relative gene expression was calculated with the ΔΔCt method.

Senescence-associated beta-galactosidase staining

Cells were washed twice with PBS and fixed with 0.5% glutaraldehyde and 1% formalin in Milli-Q water. Then the cells were washed with Milli-Q water and incubated for 24 h at 37°C with freshly made X-gal solution (0.5% X-gal, 5 mM potassium ferricyanide, 5 mM potassium ferrocyanide, 2mM MgCl2, 150mM NaCl, 7mM C6H8O7, 25mM Na2HPO4). Cells were counterstained with pararosaniline (1:25 in Milli-Q water) and detected with bright field microscopy. For each condition two independent researchers blinded to the experimental plan, scored at least 300 cells as 'negative', 'low positive', or 'high positive' (**Fig EV2**).

Bioenergetics Assays

Mitochondrial respiration was measured as oxygen consumption rate (OCR) using a XF-24 Extracellular Flux Analyzer (Seahorse Bioscience) as previously described (Milanese et al., 2019). MSCs were seeded at a density of 3×10^4 cells/well on Seahorse plates. Optimal cell densities were determined experimentally to ensure a proportional response to FCCP (**Fig EV4B-C**). 24 h after cell seeding, the medium was changed to unbuffered DMEM (XF Assay Medium-Agilent Technologies,

bioRxiv preprint doi: https://doi.org/10.1101/2020.10.11.335448; this version posted October 11, 2020. The copyright holder for this preprint (which was not certified by peer review) is the author/funder. All rights reserved. No reuse allowed without permission.

Santa Clare, Ca, USA) with 2 mM glutamine, 10 mM glucose and 1 mM sodium pyruvate and incubated 1 h at 37° C in the absence of CO_2. Three baseline measurements were performed, followed by subsequent measurements after injections of mitochondrial toxins 1.0 µM oligomycin (ATP-synthase inhibitor), 2.0 µM fluoro-carbonyl cyanide phenylhydrazone (FCCP, oxidative phosphorylation uncoupler) and 1 µM antimycin A (complex III inhibitor). Medium and reagents were adjusted to pH 7.4 according to manufacturer's procedure. Non-mitochondrial respiration, basal respiration, proton leak, ATP production, maximal respiration and spare capacity were calculated as indicated in **Fig EV4A**: The non-mitochondrial respiration was defined as the average OCR values after antimycin A injection; basal respiration was calculated as difference between basal respiration and respiration measured after antimycin A; proton leak was calculated as difference between respiration measured after oligomycin and respiration measured after antimycin A; ATP production was calculated as difference between baseline respiration and respiration measured after oligomycin injection; maximal respiration was calculated as difference between respiration after FCCP and respiration measured after antimycin A; spare capacity was defined as difference between respiration after FCCP and baseline respiration.

Data analysis

Results are statistically analyzed using PSAW statistics 20 software (SPSS Inc., Chicago, IL, USA). The normal distribution of the data was determined using the Kolmogorov-Smirnov test. When necessary the data was a log transformed to meet the normal distribution criteria. An unpaired t-test or a linear mixed model was applied, in this model the conditions were considered as fixed parameters and the donors as random factor. P-values less than 0.05 are considered as statistically significant. The grand mean is determined by calculating the mean of the donor means with 2-6 replicates per donor.

bioRxiv preprint doi: https://doi.org/10.1101/2020.10.11.335448; this version posted October 11, 2020. The copyright holder for this preprint (which was not certified by peer review) is the author/funder. All rights reserved. No reuse allowed without permission.

Acknowledgements

The authors would like to thank Andrea Lolli for advice on the *TWIST1* silencing protocol, Eric Farrell and Janneke Witte-Bouma for access to their source of MSCs, Nicole Kops and Arielle Molina Rakos for technical assistance with the senescence-associated beta-galactosidase staining and quantification, the Marius Wernig's laboratory (Stanford School of Medicine, CA) for providing the GFP overexpression construct and the lentiviral packaging constructs and the FACS sorting facility at the Erasmus MC for support with the BD Fortessa machine. This research was financially supported by the Dutch Arthritis Society (ReumaNederland; 16-1-201) and by a TTW Perspectief grant from NWO (William Hunter Revisited; P15-23). This study is part of the Medical Delta RegMed4D program and the Erasmus Postgraduate School Molecular Medicine.

Author Contribution

CV: conception and design, collection of data, data analysis and interpretation, manuscript writing and final approval of manuscript. LA: design, collection of data, data analysis and interpretation of the cellular senescence analysis experiments, manuscript editing and final approval of manuscript. WK: collection of data, data analysis, manuscript editing and final approval of manuscript. SB: design, collection of data, data analysis and interpretation of the metabolic experiments and manuscript editing and final approval of manuscript. PM: conception and design and data interpretation of the metabolic experiments, manuscript editing and final approval of manuscript. GO and RN: conception and design, data analysis and interpretation, manuscript editing and final approval of manuscript.

Conflict of interest

The authors declare that they have no conflict of interest.

Data availability

bioRxiv preprint doi: https://doi.org/10.1101/2020.10.11.335448; this version posted October 11, 2020. The copyright holder for this preprint (which was not certified by peer review) is the author/funder. All rights reserved. No reuse allowed without permission.

309 All dataset generated for this study are available on request to the corresponding author.

bioRxiv preprint doi: https://doi.org/10.1101/2020.10.11.335448; this version posted October 11, 2020. The copyright holder for this preprint (which was not certified by peer review) is the author/funder. All rights reserved. No reuse allowed without permission.

Figure legends

Figure 1 – *TWIST1* expression is negatively associated with senescence-associated β-galactosidase. (A) Representative images of senescence-associated β-galactosidase (SA-β-gal) staining counter stained with pararosaniline of MSCs 7 days after gamma irradiation with 0 or 20 Gy. Scale bar represent 100 µm. N=9, 3 donors with 3 replicates per donor. (B) *TWIST1* mRNA levels of MSCs 7 days after gamma irradiation with 0 or 20 Gy. Data show individual data points and grand mean with N=8 (0 Gy) or N=9 (20 Gy), 3 donors with 2-3 replicates per donor, linear mixed model. (C) *TWIST1* mRNA levels of MSCs transduced with an empty overexpression lentiviral construct (Control) or a TWIST1 overexpression lentiviral construct (TWIST1) after 11 days of expansion. Data show individual data points and grand mean with N=6, 2 donors with 3 replicates per donor, linear mixed model. (D) Left panel, representative images of SA-β-gal staining counter stained with pararosaniline of MSCs transduced with an empty overexpression lentiviral control construct (Empty) or a TWIST1 overexpression lentiviral construct (TWIST1) after 11 days of expansion. Right panel, quantification of SA-β-gal staining. Bars show grand mean of percentage of SA-β-gal negative, low positive and high positive cells. N=4, 2 donors with 2 replicates per donor, linear mixed model.

Figure 2 – *TWIST1* silencing induces cellular senescence in MSCs with a specific SASP mRNA expression profile. (A) *TWIST1* mRNA levels in MSCs treated for 4 passages with scramble siRNA (Scramble) or siRNA against TWIST1 (siTWIST1). N=9, 3 donors with 3 replicates per donor, linear mixed model. (B) *P16* and *P21* mRNA levels in MSCs treated for 4 passages with scramble siRNA (Scramble) or siRNA against TWIST1 (siTWIST1). N=9, 3 donors with 3 replicates per donor, linear mixed model. (C) Quantification of senescence associated beta galactosidase (SA-β-gal) staining based on intensity (negative, low positive and high positive) of MSCs treated for 4 passages with scramble siRNA (Scramble) or siRNA against TWIST1 (siTWIST1). N=6, 3 donors with 2 replicates per donor, linear mixed model. (D) Cell number data during expansion of MSCs treated with scramble

bioRxiv preprint doi: https://doi.org/10.1101/2020.10.11.335448; this version posted October 11, 2020. The copyright holder for this preprint (which was not certified by peer review) is the author/funder. All rights reserved. No reuse allowed without permission.

siRNA (Scramble) or siRNA against TWIST1 (siTWIST1) at day 0, 3, 7, 10 and 14 of treatment, N=3 donors. (E) *IL6*, *IL10*, *IL1B*, *MMP3*, *IL8*, *CCL2* and *VEGFA* mRNA levels in MSCs treated for 4 passages with scramble siRNA (Scramble) or siRNA against TWIST1 (siTWIST1). N=9, 3 donors with 3 replicates per donor, linear mixed model. Graphs show individual data points and grand mean.

Figure 3 – Increased oxygen consumption rate (OCR) in *TWIST1* silenced MSCs. (A-B) Graph shows the OCR in MSCs treated with a scramble or TWIST1 siRNA at basal level and after addition of oligomycin, FCCP and antimycin A in two different donors MSC-6 (A) and MSC-7 (B). Values represent mean with SD, N=3-5 replicates per donor. (C-H) Graphs show calculated values for basal OCR (C), maximum OCR (D), proton leak (E), ATP production (F), spare capacity (G) and non-mitochondrial respiration (H) in MSCs treated with scramble or TWIST1 siRNA. N=6-9, 2 donors with 3-5 replicates per donor, linear mixed model. Graphs show individual data points and grand mean.

Figure 4 –*TWIST1* silencing did not increases extracellular acidification rate (ECAR) in MSCs. (A-B) Graph shows the ECAR in MSCs treated with a scramble or TWIST1 siRNA at basal level and after addition of oligomycin, FCCP and antimycin A in two different donors MSC-6 (A) and MSC-7 (B). Values represent mean with SD, N=3-5 replicates per donor. (C) Graphs show ECAR values for basal OCR and maximum OCR in MSCs treated with scramble or TWIST1 siRNA. N=6-9, 2 donors with 3-5 replicates per donor, linear mixed model. Graphs show individual data points and grand mean.

Figure 5 - Schematic overview of the characteristics of *TWIST1* silencing-induced senescence and irradiation-induced senescence. Both *TWIST1* silencing-induced and irradiation-induced senescence stimulated senescence-associated beta-galactosidase (SA-β-gal) activity in MSCs, decreased their expansion rate and induced high levels of *P16* and *P21* mRNA. *TWIST1* silencing-induced senescence,

bioRxiv preprint doi: https://doi.org/10.1101/2020.10.11.335448; this version posted October 11, 2020. The copyright holder for this preprint (which was not certified by peer review) is the author/funder. All rights reserved. No reuse allowed without permission.

359 however, increased oxygen respiration in MSCs, increased the expression of the SASP related genes
360 *CCL2* and *IL1B,* and lack the expression of *IL8*, *IL6, IL10, MMP3* and *VEGFA.* Irradiation-induced
361 senescent MSCs showed increased oxygen respiration, increased glycolytic flux and classical SASP
362 expression.

363

364 **References**

365 Bittles, A.H., and Harper, N. (1984). Increased glycolysis in ageing cultured human diploid fibroblasts.
366 Biosci Rep *4*, 751-756.
367 Boregowda, S.V., Krishnappa, V., Haga, C.L., Ortiz, L.A., and Phinney, D.G. (2016). A Clinical
368 Indications Prediction Scale Based on TWIST1 for Human Mesenchymal Stem Cells. EBioMedicine *4*,
369 62-73.
370 Brookes, P.S. (2005). Mitochondrial H(+) leak and ROS generation: an odd couple. Free Radic Biol
371 Med *38*, 12-23.
372 Burns, T.F., Dobromilskaya, I., Murphy, S.C., Gajula, R.P., Thiyagarajan, S., Chatley, S.N., Aziz, K., Cho,
373 Y.J., Tran, P.T., and Rudin, C.M. (2013). Inhibition of TWIST1 leads to activation of oncogene-induced
374 senescence in oncogene-driven non-small cell lung cancer. Mol Cancer Res *11*, 329-338.
375 Cheng, H., Qiu, L., Ma, J., Zhang, H., Cheng, M., Li, W., Zhao, X., and Liu, K. (2011). Replicative
376 senescence of human bone marrow and umbilical cord derived mesenchymal stem cells and their
377 differentiation to adipocytes and osteoblasts. Mol Biol Rep *38*, 5161-5168.
378 Correia-Melo, C., Marques, F.D., Anderson, R., Hewitt, G., Hewitt, R., Cole, J., Carroll, B.M., Miwa, S.,
379 Birch, J., Merz, A.*, et al.* (2016). Mitochondria are required for pro-ageing features of the senescent
380 phenotype. Embo J *35*, 724-742.
381 Dörr, J.R., Yu, Y., Milanovic, M., Beuster, G., Zasada, C., Däbritz, J.H., Lisec, J., Lenze, D., Gerhardt, A.,
382 Schleicher, K.*, et al.* (2013). Synthetic lethal metabolic targeting of cellular senescence in cancer
383 therapy. Nature *501*, 421-425.

bioRxiv preprint doi: https://doi.org/10.1101/2020.10.11.335448; this version posted October 11, 2020. The copyright holder for this preprint (which was not certified by peer review) is the author/funder. All rights reserved. No reuse allowed without permission.

384 Erices, A., Conget, P., and Minguell, J.J. (2000). Mesenchymal progenitor cells in human umbilical
385 cord blood. Br J Haematol *109*, 235-242.
386 Halvorsen, Y.C., Wilkison, W.O., and Gimble, J.M. (2000). Adipose-derived stromal cells--their utility
387 and potential in bone formation. Int J Obes Relat Metab Disord *24 Suppl 4*, S41-44.
388 Haynesworth, S.E., Goshima, J., Goldberg, V.M., and Caplan, A.I. (1992). Characterization of cells with
389 osteogenic potential from human marrow. Bone *13*, 81-88.
390 Hochane, M., Trichet, V., Pecqueur, C., Avril, P., Oliver, L., Denis, J., Brion, R., Amiaud, J., Pineau, A.,
391 Naveilhan, P.*, et al.* (2017). Low-Dose Pesticide Mixture Induces Senescence in Normal Mesenchymal
392 Stem Cells (MSC) and Promotes Tumorigenic Phenotype in Premalignant MSC. Stem Cells *35*, 800-
393 811.
394 Isenmann, S., Arthur, A., Zannettino, A.C., Turner, J.L., Shi, S., Glackin, C.A., and Gronthos, S. (2009).
395 TWIST family of basic helix-loop-helix transcription factors mediate human mesenchymal stem cell
396 growth and commitment. Stem Cells *27*, 2457-2468.
397 James, E.L., Michalek, R.D., Pitiyage, G.N., de Castro, A.M., Vignola, K.S., Jones, J., Mohney, R.P.,
398 Karoly, E.D., Prime, S.S., and Parkinson, E.K. (2015). Senescent human fibroblasts show increased
399 glycolysis and redox homeostasis with extracellular metabolomes that overlap with those of
400 irreparable DNA damage, aging, and disease. J Proteome Res *14*, 1854-1871.
401 Knuth, C.A., Kiernan, C.H., Palomares Cabeza, V., Lehmann, J., Witte-Bouma, J., Ten Berge, D., Brama,
402 P.A., Wolvius, E.B., Strabbing, E.M., Koudstaal, M.J.*, et al.* (2018). Isolating Pediatric Mesenchymal
403 Stem Cells with Enhanced Expansion and Differentiation Capabilities. Tissue Eng Part C Methods *24*,
404 313-321.
405 Lee, H.C., Yin, P.H., Chi, C.W., and Wei, Y.H. (2002). Increase in mitochondrial mass in human
406 fibroblasts under oxidative stress and during replicative cell senescence. J Biomed Sci *9*, 517-526.
407 Li, Y., Wu, Q., Wang, Y., Li, L., Bu, H., and Bao, J. (2017). Senescence of mesenchymal stem cells
408 (Review). Int J Mol Med *39*, 775-782.

bioRxiv preprint doi: https://doi.org/10.1101/2020.10.11.335448; this version posted October 11, 2020. The copyright holder for this preprint (which was not certified by peer review) is the author/funder. All rights reserved. No reuse allowed without permission.

409 Li, Y., Xu, X., Wang, L., Liu, G., Li, Y., Wu, X., Jing, Y., Li, H., and Wang, G. (2015). Senescent
410 mesenchymal stem cells promote colorectal cancer cells growth via galectin-3 expression. Cell Biosci
411 *5*, 21.
412 Loeser, R.F., Collins, J.A., and Diekman, B.O. (2016). Ageing and the pathogenesis of osteoarthritis.
413 Nat Rev Rheumatol *12*, 412-420.
414 Lu, S., Wang, H., Ren, R., Shi, X., Zhang, Y., and Ma, W. (2018). Reduced expression of Twist 1 is
415 protective against insulin resistance of adipocytes and involves mitochondrial dysfunction. Sci Rep *8*,
416 12590.
417 Lunyak, V.V., Amaro-Ortiz, A., and Gaur, M. (2017). Mesenchymal Stem Cells Secretory Responses:
418 Senescence Messaging Secretome and Immunomodulation Perspective. Front Genet *8*, 220.
419 Milanese, C., Bombardieri, C.R., Sepe, S., Barnhoorn, S., Payán-Goméz, C., Caruso, D., Audano, M.,
420 Pedretti, S., Vermeij, W.P., Brandt, R.M.C*., et al.* (2019). DNA damage and transcription stress cause
421 ATP-mediated redesign of metabolism and potentiation of anti-oxidant buffering. Nat Commun *10*,
422 4887.
423 Narcisi, R., Cleary, M.A., Brama, P.A., Hoogduijn, M.J., Tuysuz, N., ten Berge, D., and van Osch, G.J.
424 (2015). Long-term expansion, enhanced chondrogenic potential, and suppression of endochondral
425 ossification of adult human MSCs via WNT signaling modulation. Stem Cell Reports *4*, 459-472.
426 Nayak, D., Kumar, A., Chakraborty, S., Rasool, R.U., Amin, H., Katoch, A., Gopinath, V., Mahajan, V.,
427 Zilla, M.K., Rah, B*., et al.* (2017). Inhibition of Twist1-mediated invasion by Chk2 promotes premature
428 senescence in p53-defective cancer cells. Cell Death Differ *24*, 1275-1287.
429 Pattappa, G., Heywood, H.K., de Bruijn, J.D., and Lee, D.A. (2011). The metabolism of human
430 mesenchymal stem cells during proliferation and differentiation. J Cell Physiol *226*, 2562-2570.
431 Pittenger, M.F., Mackay, A.M., Beck, S.C., Jaiswal, R.K., Douglas, R., Mosca, J.D., Moorman, M.A.,
432 Simonetti, D.W., Craig, S., and Marshak, D.R. (1999). Multilineage potential of adult human
433 mesenchymal stem cells. Science *284*, 143-147.

bioRxiv preprint doi: https://doi.org/10.1101/2020.10.11.335448; this version posted October 11, 2020. The copyright holder for this preprint (which was not certified by peer review) is the author/funder. All rights reserved. No reuse allowed without permission.

Quijano, C., Cao, L., Fergusson, M.M., Romero, H., Liu, J., Gutkind, S., Rovira, II, Mohney, R.P., Karoly, E.D., and Finkel, T. (2012). Oncogene-induced senescence results in marked metabolic and bioenergetic alterations. Cell Cycle *11*, 1383-1392.

Romanov, Y.A., Svintsitskaya, V.A., and Smirnov, V.N. (2003). Searching for alternative sources of postnatal human mesenchymal stem cells: candidate MSC-like cells from umbilical cord. Stem Cells *21*, 105-110.

Seo, S.K., Kim, J.H., Choi, H.N., Choe, T.B., Hong, S.I., Yi, J.Y., Hwang, S.G., Lee, H.G., Lee, Y.H., and Park, I.C. (2014). Knockdown of TWIST1 enhances arsenic trioxide- and ionizing radiation-induced cell death in lung cancer cells by promoting mitochondrial dysfunction. Biochem Biophys Res Commun *449*, 490-495.

Tran, P.T., Shroff, E.H., Burns, T.F., Thiyagarajan, S., Das, S.T., Zabuawala, T., Chen, J., Cho, Y.J., Luong, R., Tamayo, P.*, et al.* (2012). Twist1 suppresses senescence programs and thereby accelerates and maintains mutant Kras-induced lung tumorigenesis. PLoS Genet *8*, e1002650.

Tsai, C.C., Chen, Y.J., Yew, T.L., Chen, L.L., Wang, J.Y., Chiu, C.H., and Hung, S.C. (2011). Hypoxia inhibits senescence and maintains mesenchymal stem cell properties through down-regulation of E2A-p21 by HIF-TWIST. Blood *117*, 459-469.

Vizioli, M.G., Liu, T., Miller, K.N., Robertson, N.A., Gilroy, K., Lagnado, A.B., Perez-Garcia, A., Kiourtis, C., Dasgupta, N., Lei, X.*, et al.* (2020). Mitochondria-to-nucleus retrograde signaling drives formation of cytoplasmic chromatin and inflammation in senescence. Genes Dev *34*, 428-445.

Voskamp, C., van de Peppel, J., Gasparini, S., Giannoni, P., van Leeuwen, J., van Osch, G., and Narcisi, R. (2020). Sorting living mesenchymal stem cells using a TWIST1 RNA-based probe depends on incubation time and uptake capacity. Cytotechnology *72*, 37-45.

Wiley, C.D., Velarde, M.C., Lecot, P., Liu, S., Sarnoski, E.A., Freund, A., Shirakawa, K., Lim, H.W., Davis, S.S., Ramanathan, A.*, et al.* (2016). Mitochondrial Dysfunction Induces Senescence with a Distinct Secretory Phenotype. Cell Metab *23*, 303-314.

bioRxiv preprint doi: https://doi.org/10.1101/2020.10.11.335448; this version posted October 11, 2020. The copyright holder for this preprint (which was not certified by peer review) is the author/funder. All rights reserved. No reuse allowed without permission.

459 Xu, M., Bradley, E.W., Weivoda, M.M., Hwang, S.M., Pirtskhalava, T., Decklever, T., Curran, G.L.,
460 Ogrodnik, M., Jurk, D., Johnson, K.O*., et al.* (2017). Transplanted Senescent Cells Induce an
461 Osteoarthritis-Like Condition in Mice. J Gerontol A Biol Sci Med Sci *72*, 780-785.
462 Zhu, Y., Armstrong, J.L., Tchkonia, T., and Kirkland, J.L. (2014). Cellular senescence and the senescent
463 secretory phenotype in age-related chronic diseases. Curr Opin Clin Nutr Metab Care *17*, 324-328.
464 Zuk, P.A., Zhu, M., Mizuno, H., Huang, J., Futrell, J.W., Katz, A.J., Benhaim, P., Lorenz, H.P., and
465 Hedrick, M.H. (2001). Multilineage cells from human adipose tissue: implications for cell-based
466 therapies. Tissue Eng *7*, 211-228.

467

bioRxiv preprint doi: https://doi.org/10.1101/2020.10.11.335448; this version posted October 11, 2020. The copyright holder for this preprint (which was not certified by peer review) is the author/funder. All rights reserved. No reuse allowed without permission.

A

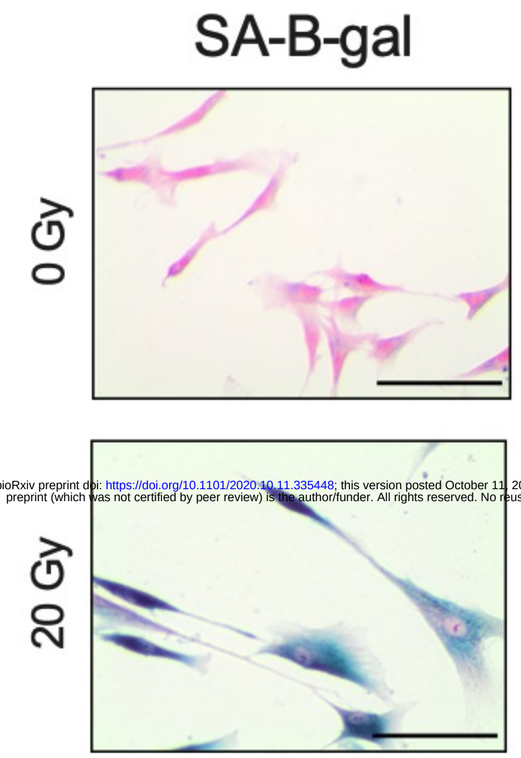

B

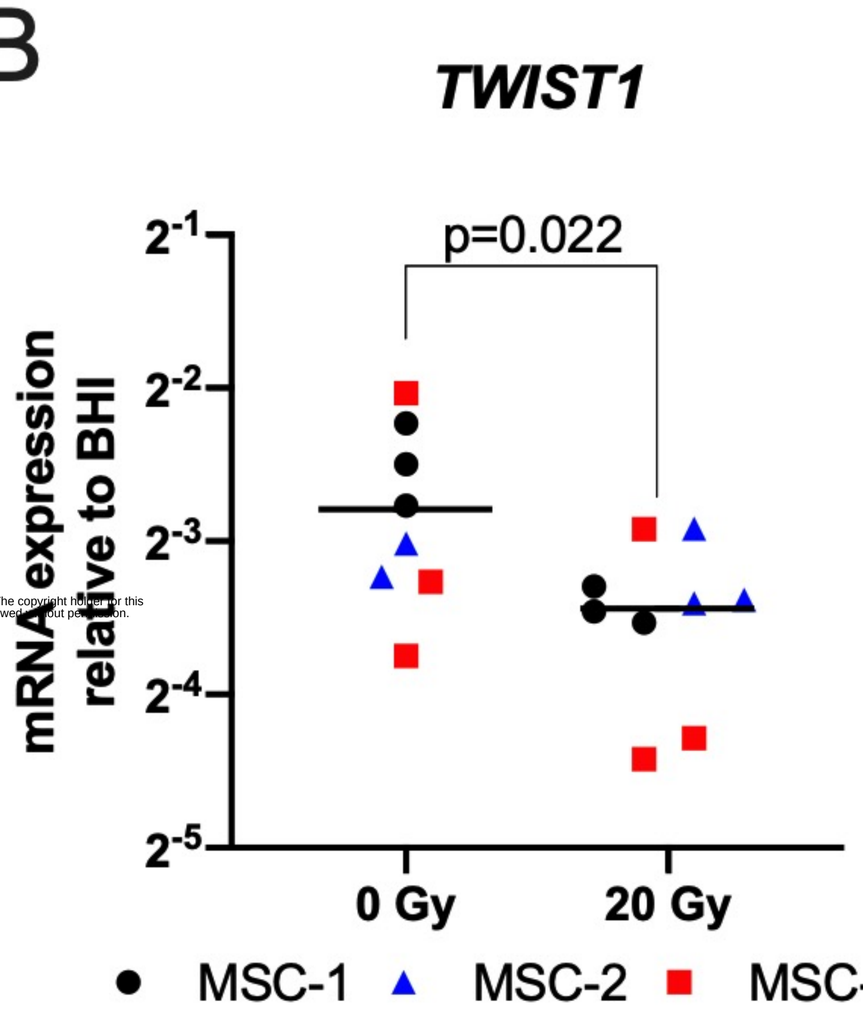

C

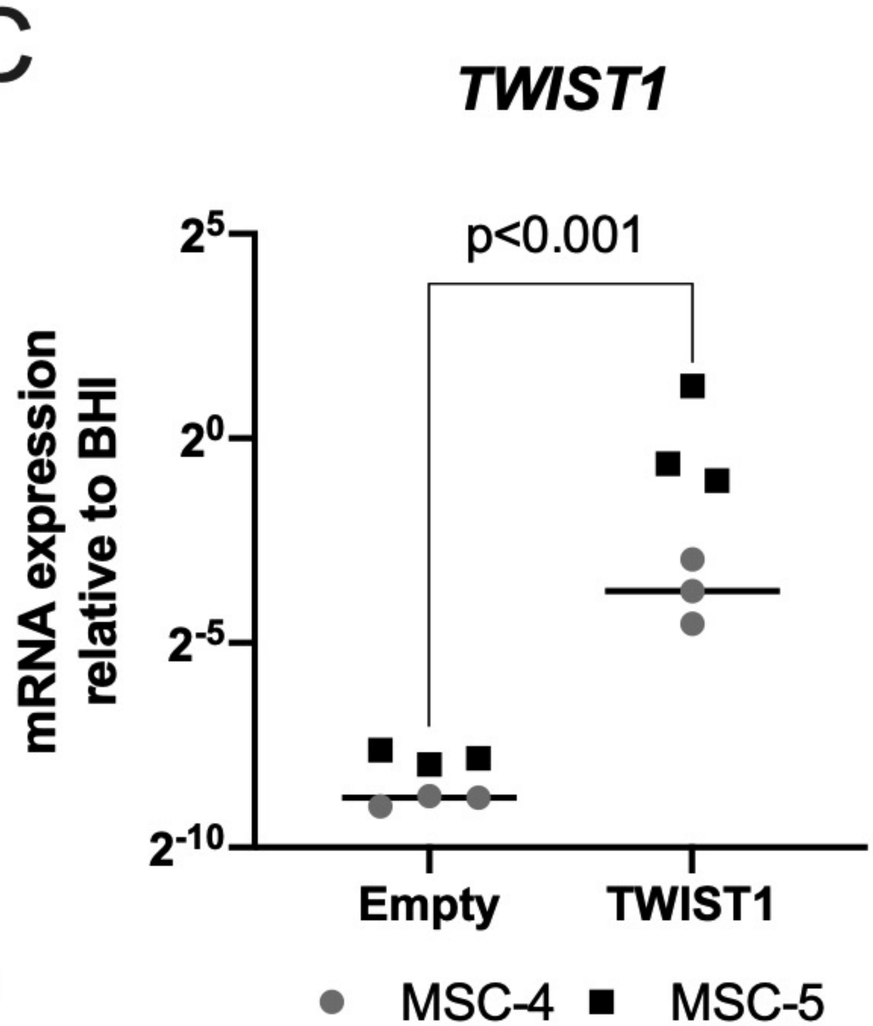

D

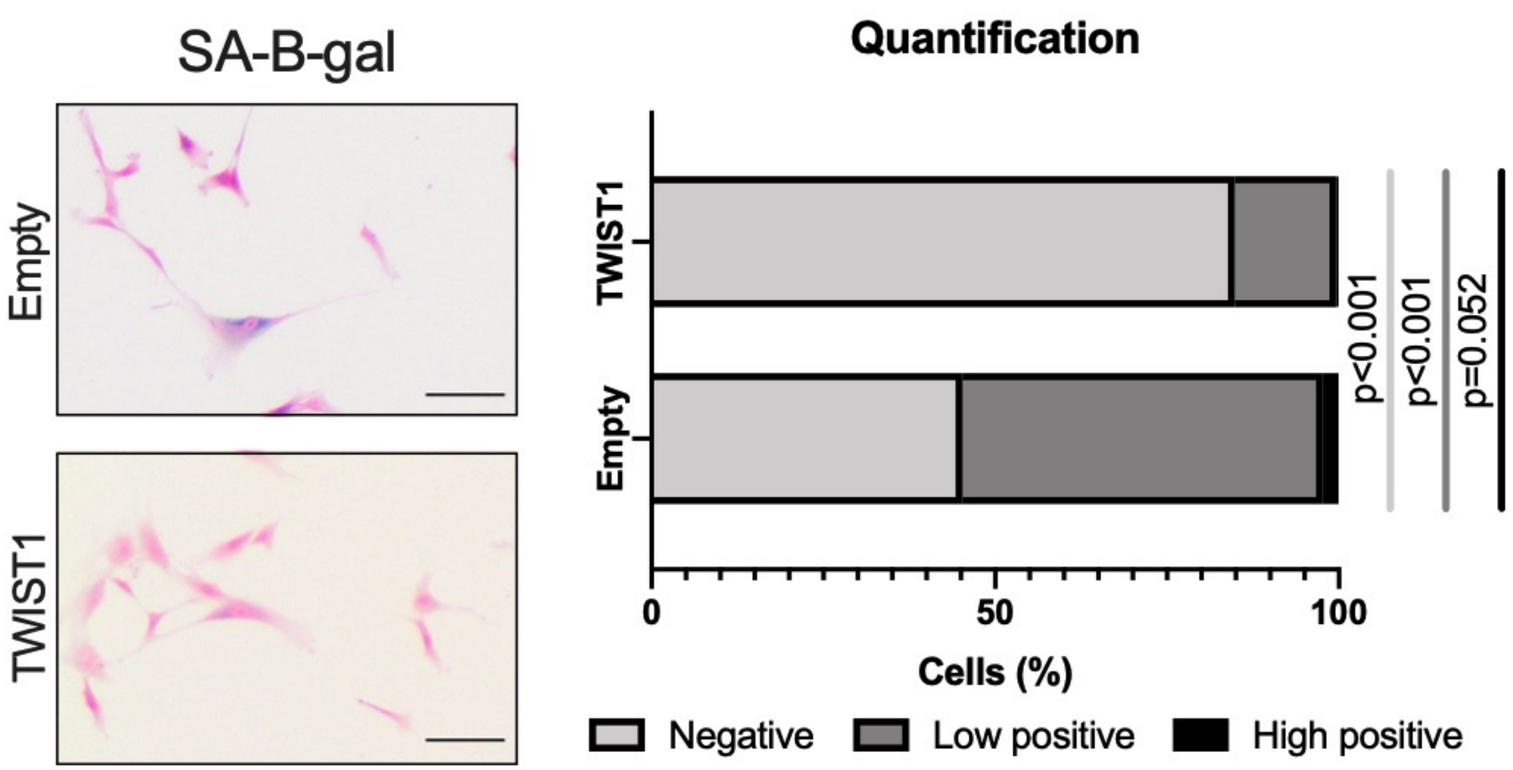

A

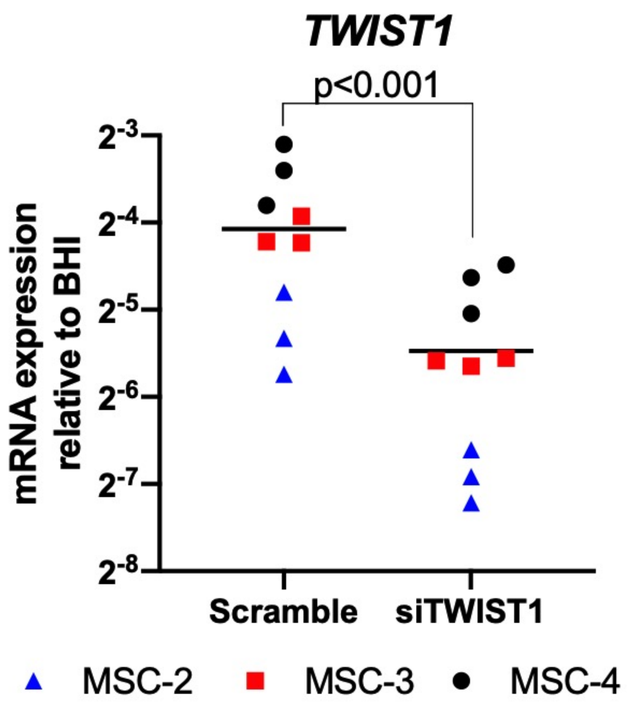

B

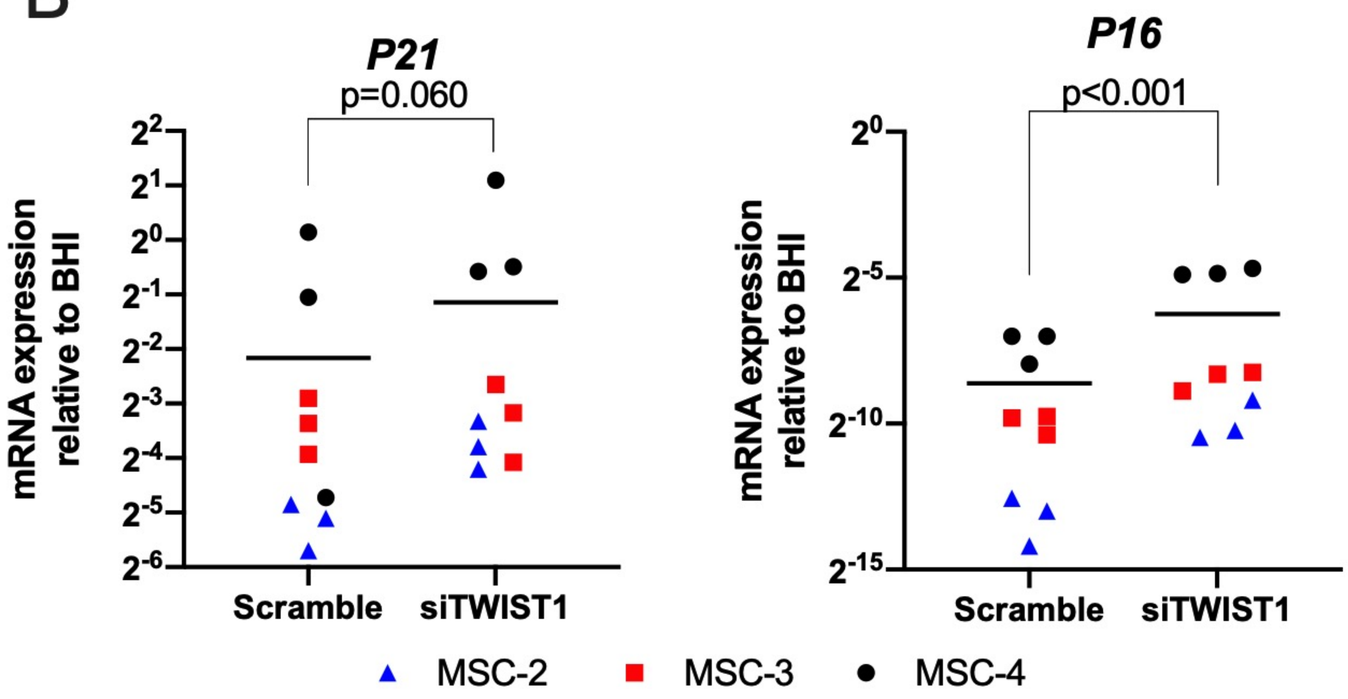

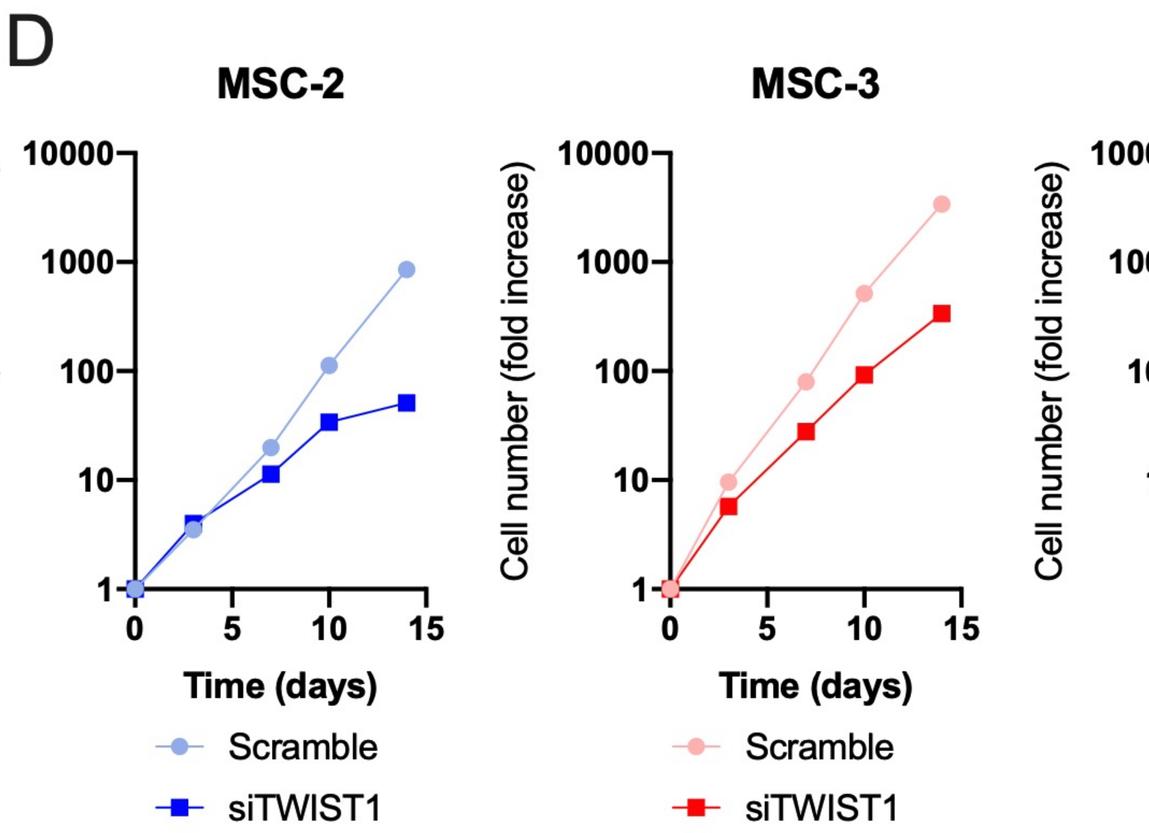

C

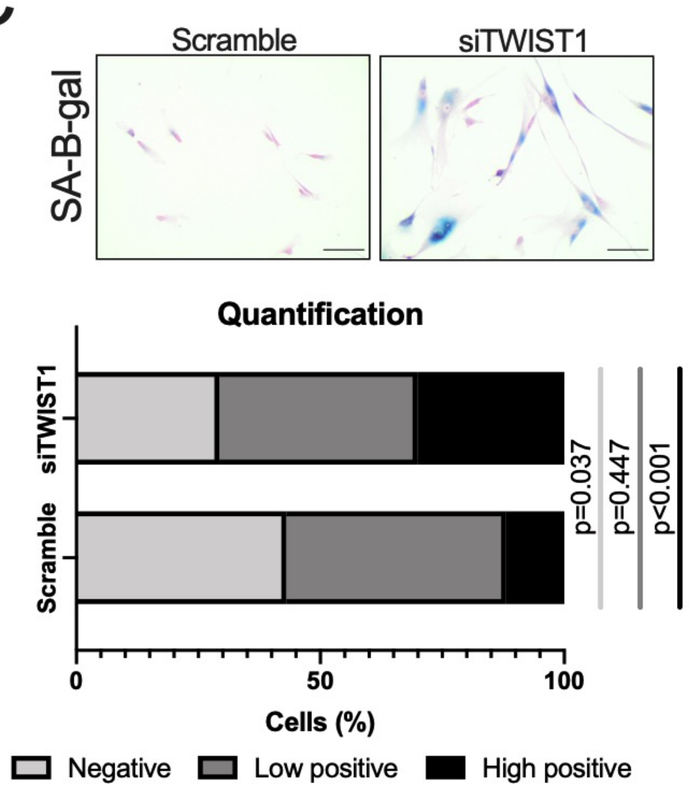

D

E

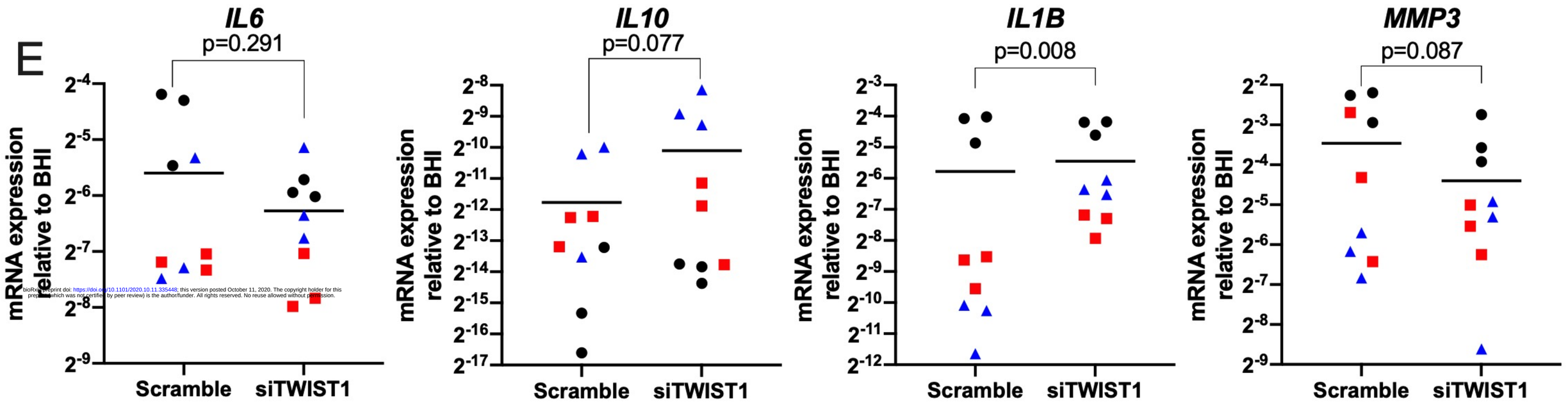

bioRxiv preprint doi: https://doi.org/10.1101/2020.10.11.335448; this version posted October 11, 2020. The copyright holder for this preprint (which was not certified by peer review) is the author/funder. All rights reserved. No reuse allowed without permission.

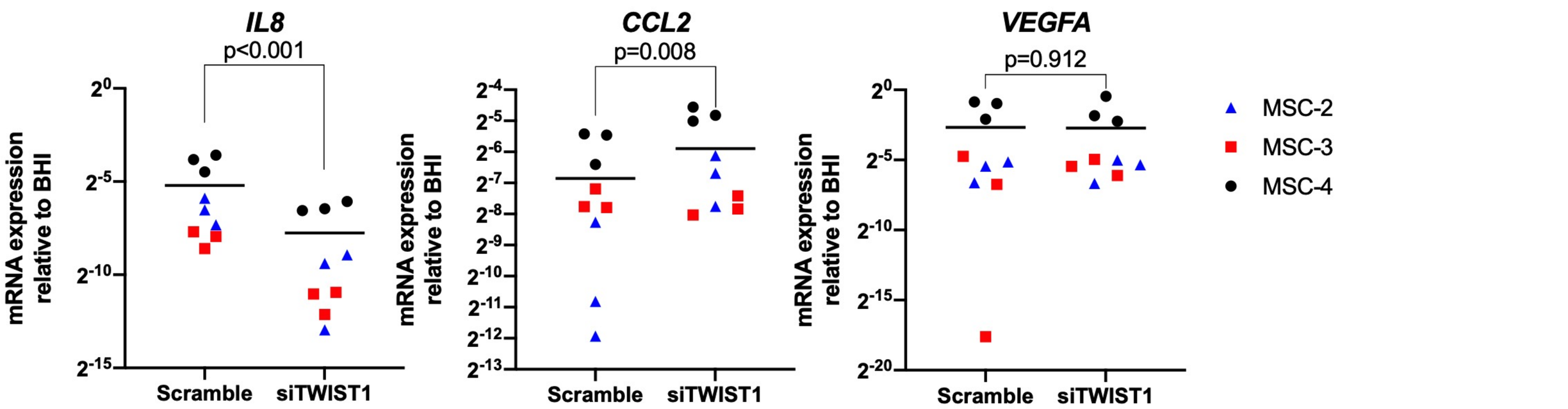

bioRxiv preprint doi: https://doi.org/10.1101/2020.10.11.335448; this version posted October 11, 2020. The copyright holder for this preprint (which was not certified by peer review) is the author/funder. All rights reserved. No reuse allowed without permission.

A

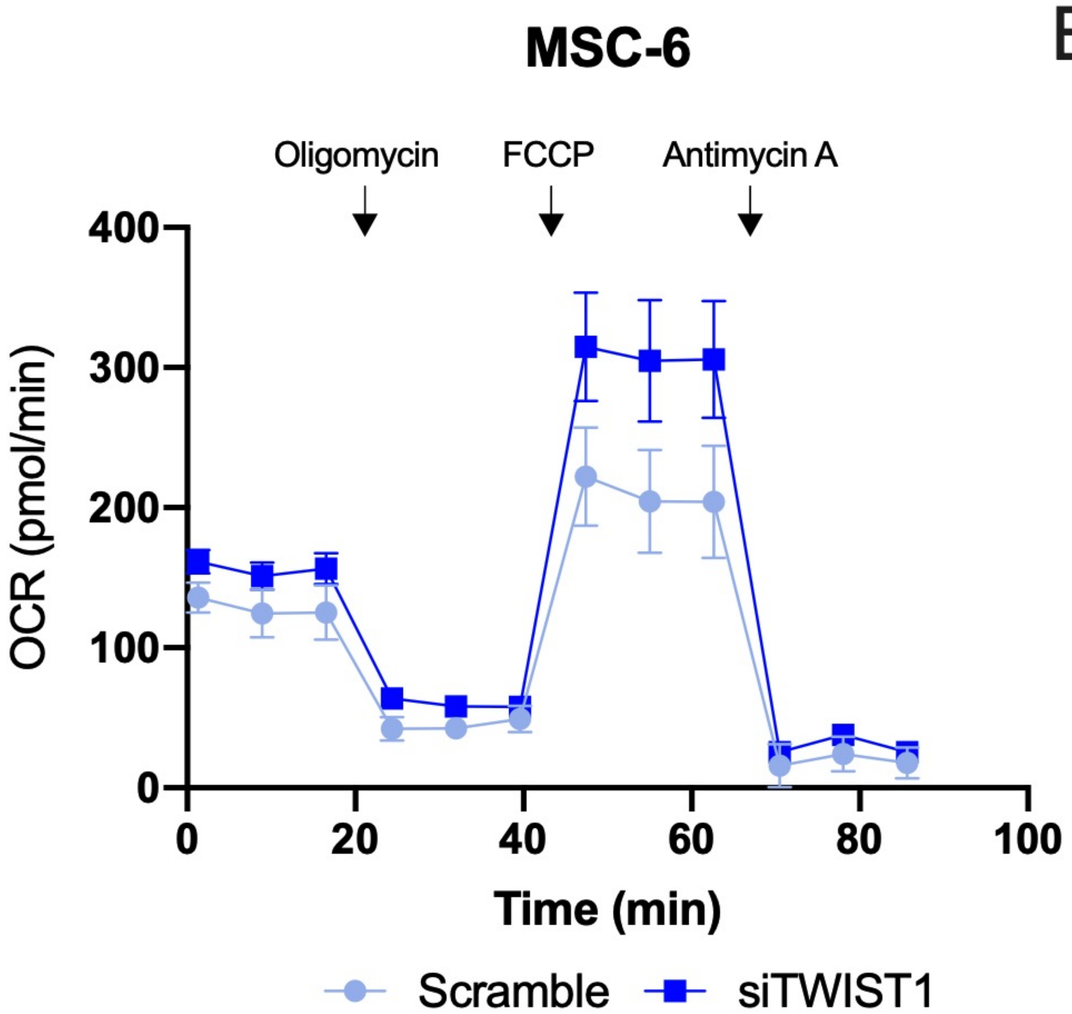

B

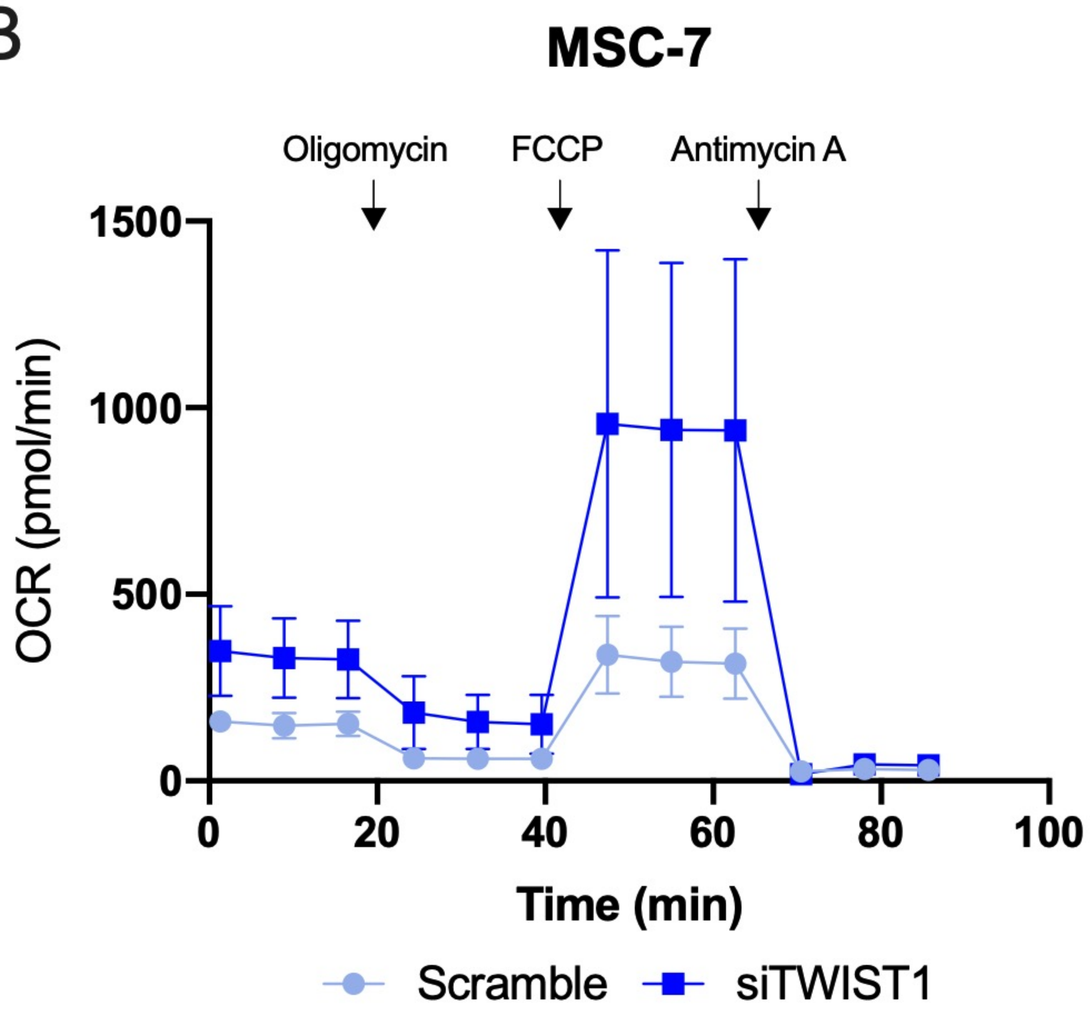

C

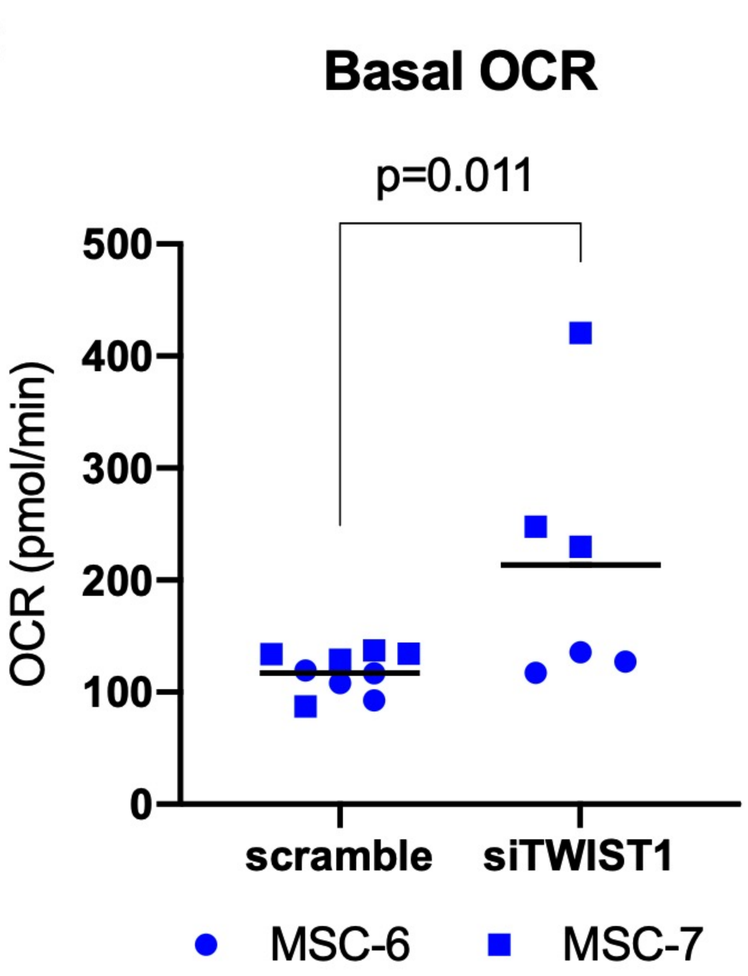

D

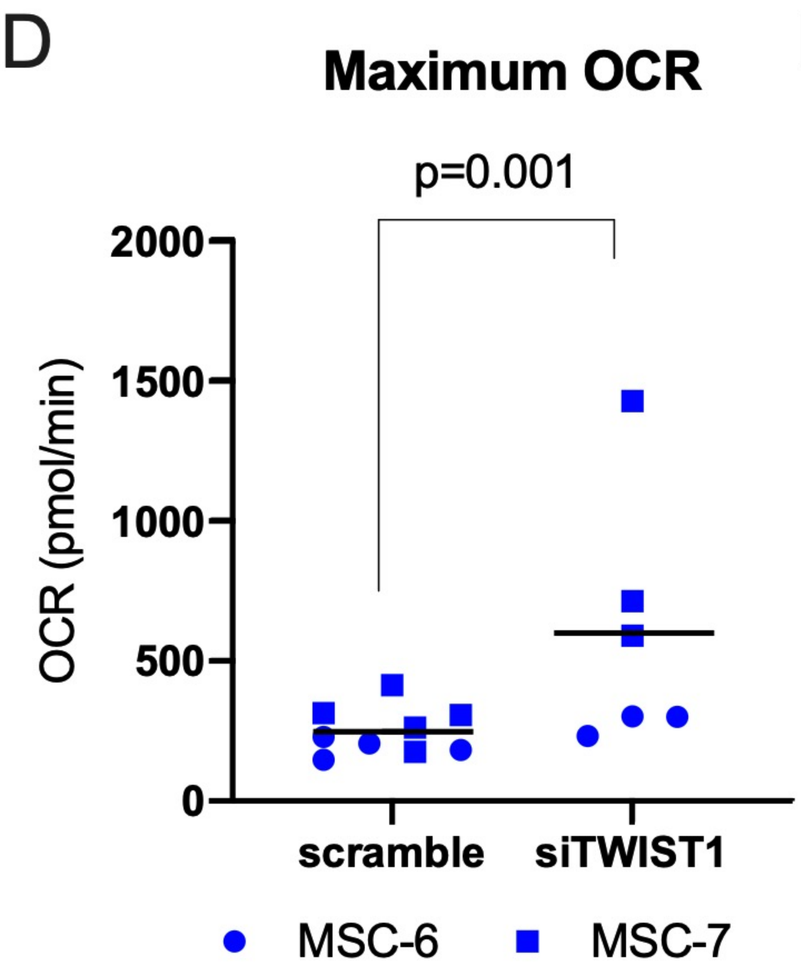

E

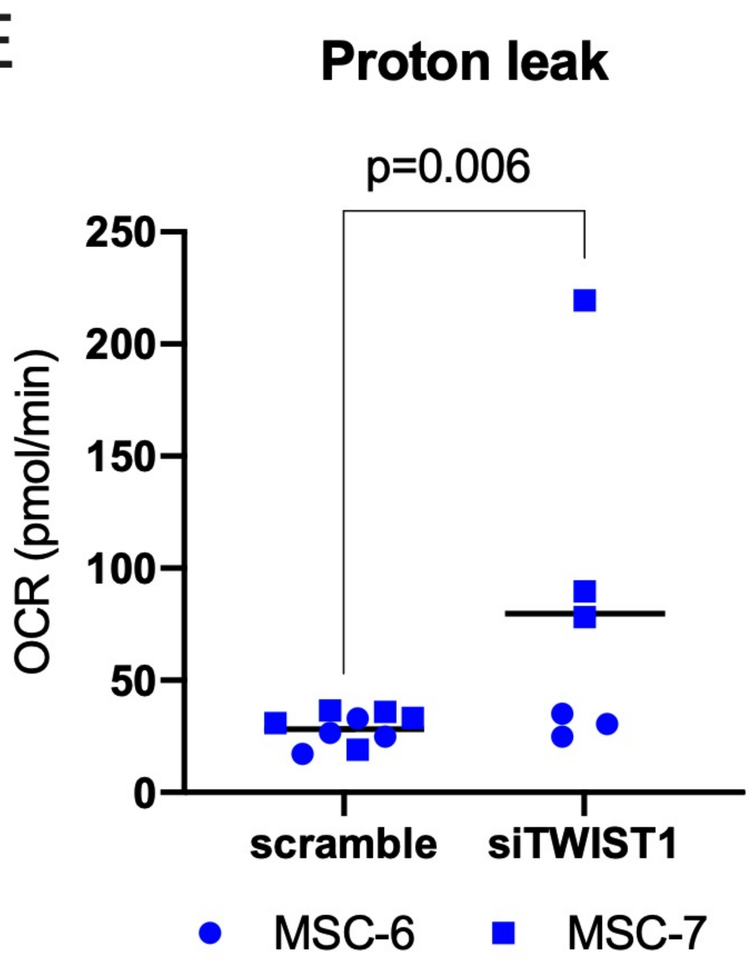

F

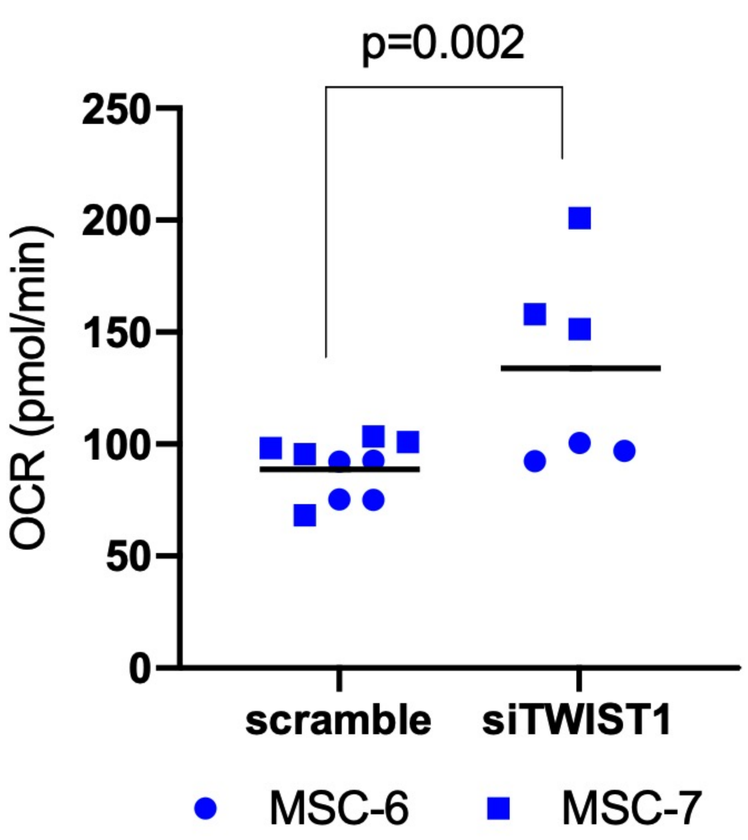

G

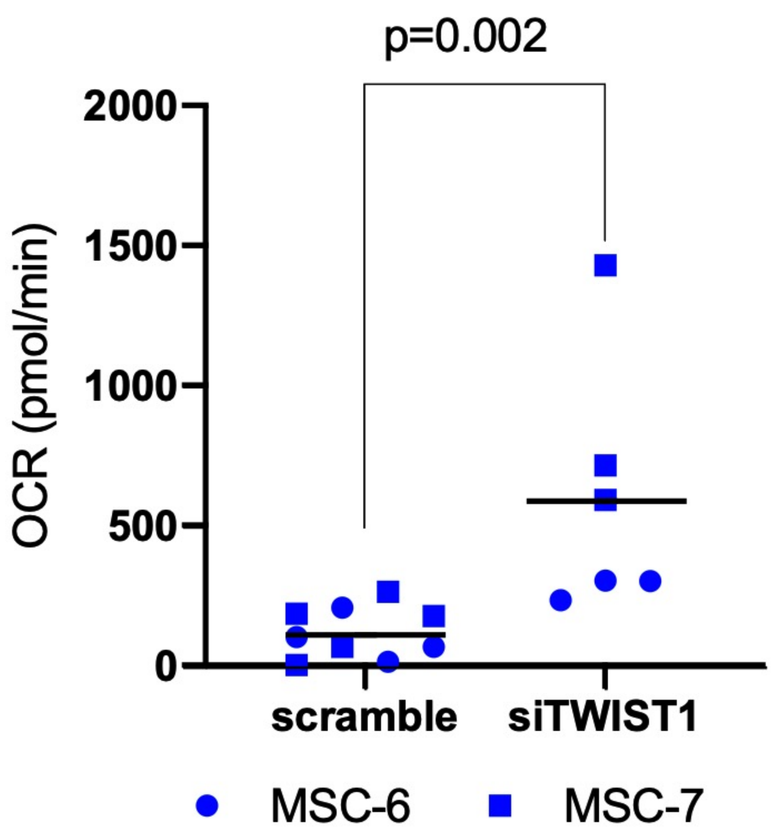

H

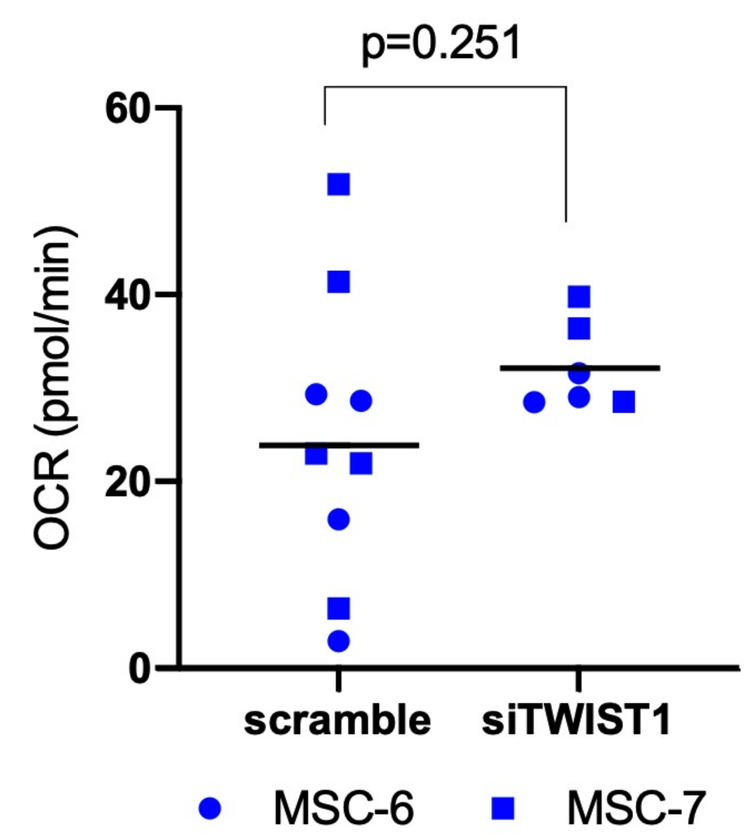

bioRxiv preprint doi: https://doi.org/10.1101/2020.10.11.335448; this version posted October 11, 2020. The copyright holder for this preprint (which was not certified by peer review) is the author/funder. All rights reserved. No reuse allowed without permission.

A

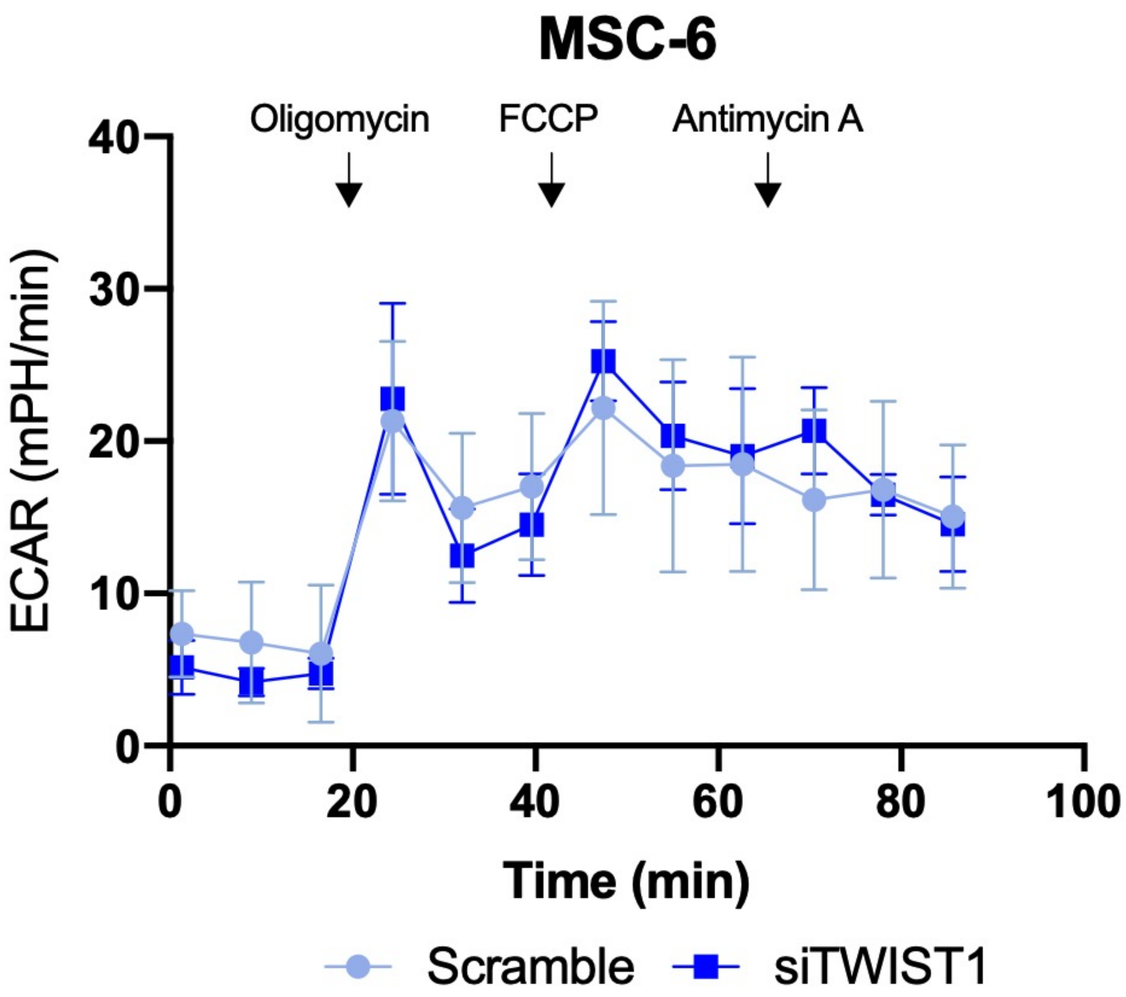

B

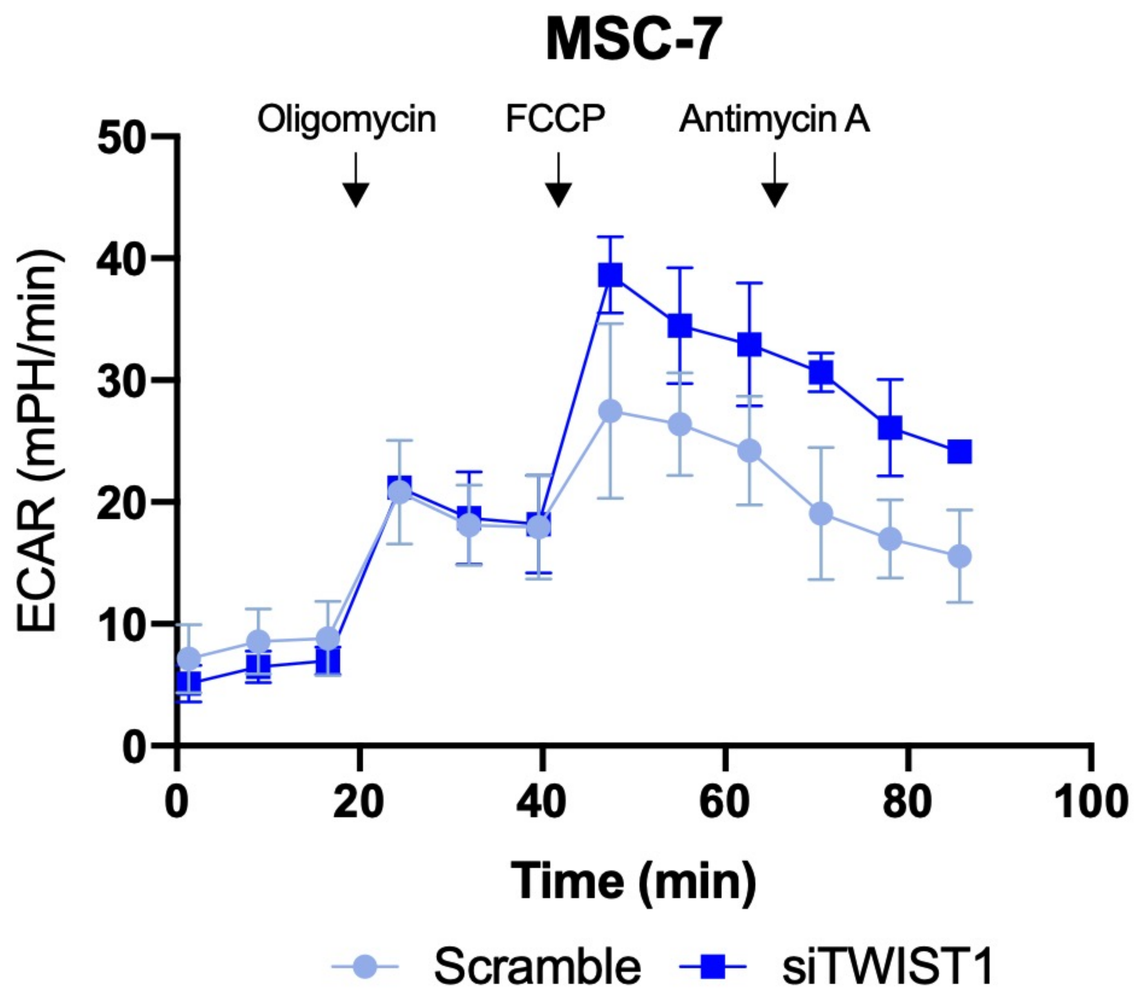

C

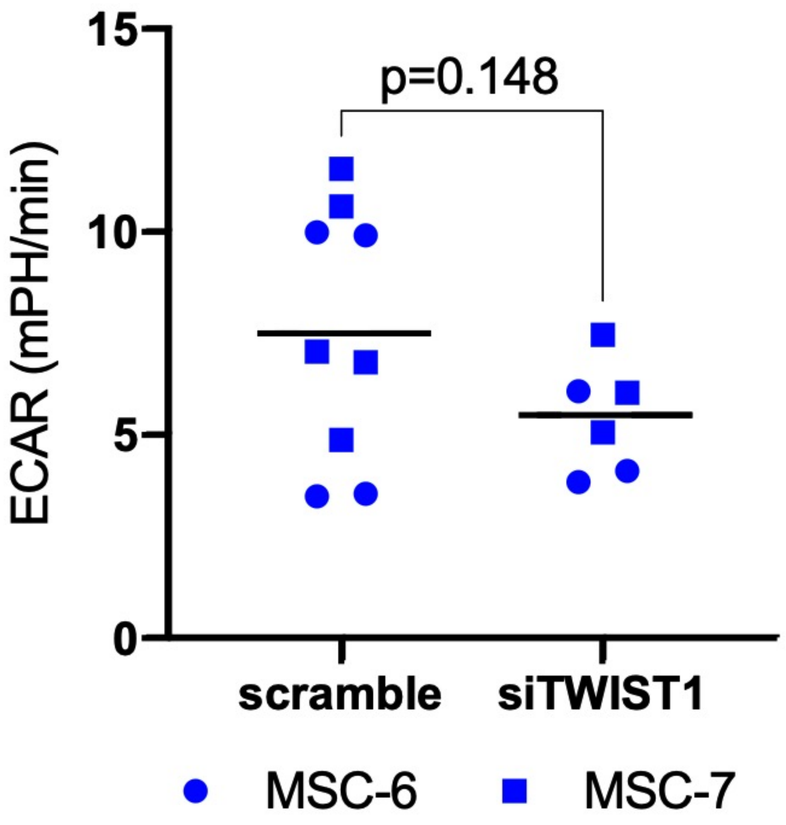

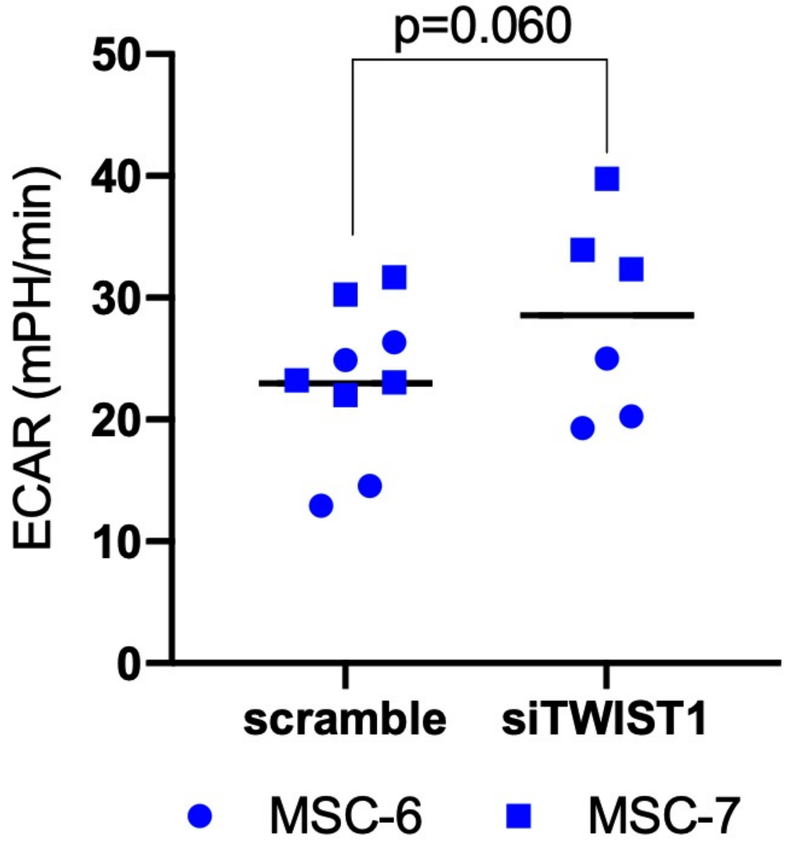

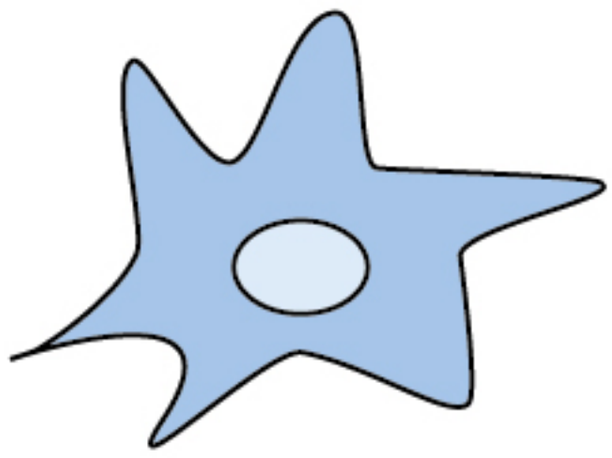

TWIST1-silenced induced senescence

- *CCL2* and *IL1B* expression
- Increased respiration

- High SA-β-Gal activity
- Growth arrest
- Increased expression of *P16* and *P21*

- Increased respiration
- Increased glycolytic flux
- Classical SASP expression

Irradiation induced senescence

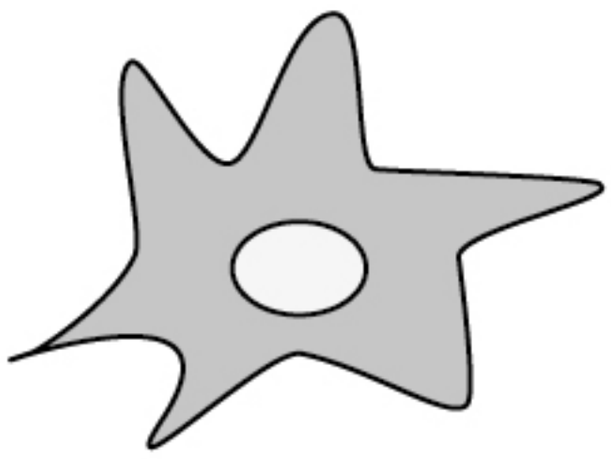

bioRxiv preprint doi: https://doi.org/10.1101/2020.10.11.335448; this version posted October 11, 2020. The copyright holder for this preprint (which was not certified by peer review) is the author/funder. All rights reserved. No reuse allowed without permission.

bioRxiv preprint doi: https://doi.org/10.1101/2020.10.11.335448; this version posted October 11, 2020. The copyright holder for this preprint (which was not certified by peer review) is the author/funder. All rights reserved. No reuse allowed without permission.

Expanded view Figures

bioRxiv preprint doi: https://doi.org/10.1101/2020.10.11.335448; this version posted October 11, 2020. The copyright holder for this preprint (which was not certified by peer review) is the author/funder. All rights reserved. No reuse allowed without permission.

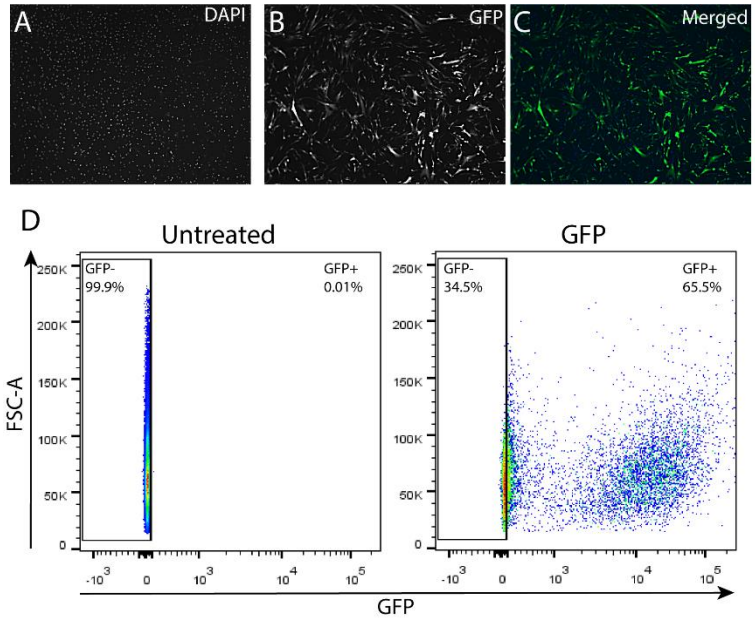

Fig EV1. Related to Fig1. More than 65% of the MSCs were transduced using a GFP overexpression lentivirus. (A-C) Representative fluorescent microscope images of GFP lentivirus transduced MSCs stained with DAPI (nuclei), N=1 donor. (D) Flowcytometry graphs of untreated MSCs and MSCs transduced with the GFP lentivirus, N=1 donor.

bioRxiv preprint doi: https://doi.org/10.1101/2020.10.11.335448; this version posted October 11, 2020. The copyright holder for this preprint (which was not certified by peer review) is the author/funder. All rights reserved. No reuse allowed without permission.

A

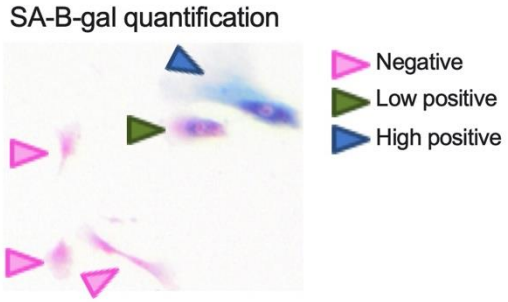

B

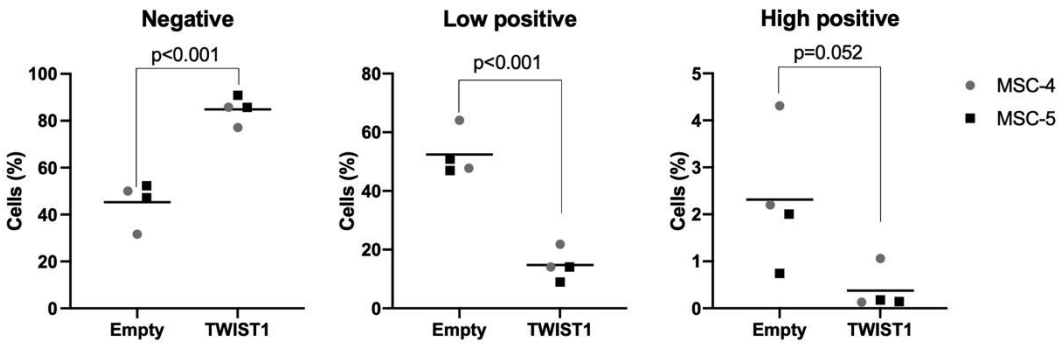

C

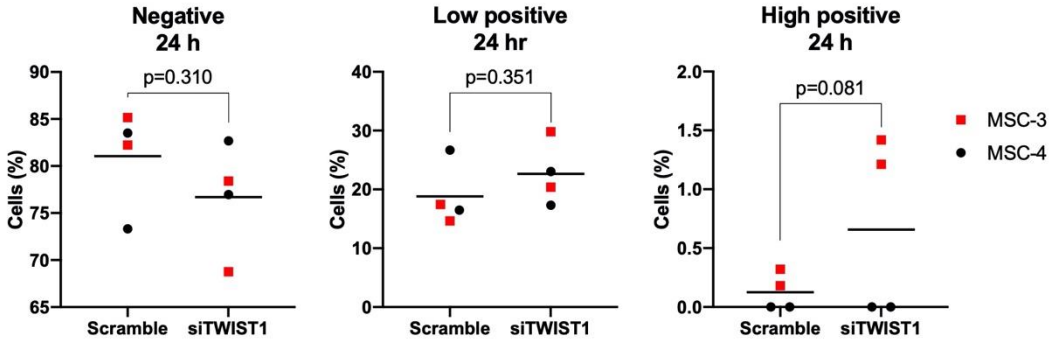

D

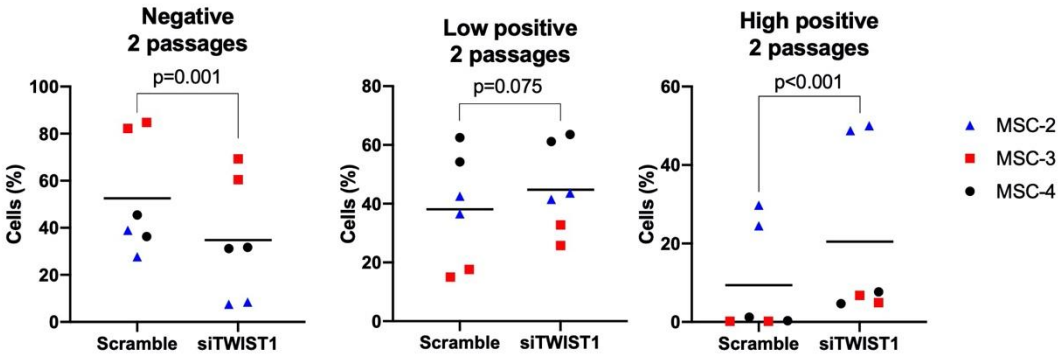

E

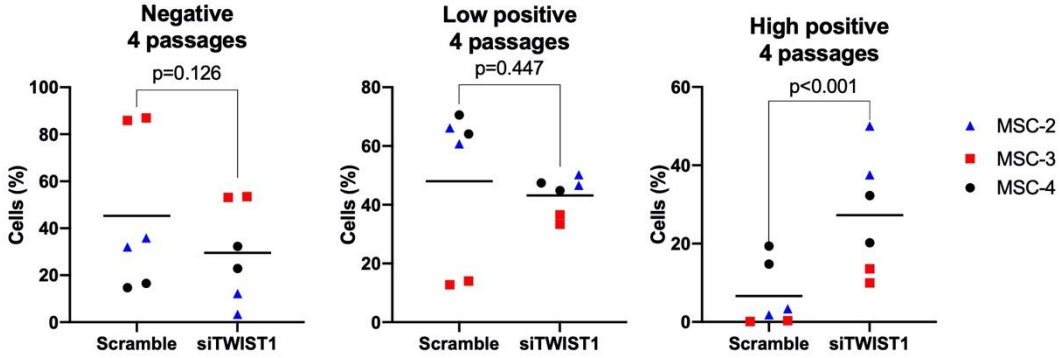

bioRxiv preprint doi: https://doi.org/10.1101/2020.10.11.335448; this version posted October 11, 2020. The copyright holder for this preprint (which was not certified by peer review) is the author/funder. All rights reserved. No reuse allowed without permission.

Fig EV2. Related to Fig1 and Fig 2. Quantification of senescence-associated β-galactosidase staining in low positive, high positive or negative cells. (A) MSCs were categorized as negative for senescence-associated β-galactosidase (SA-β-gal) staining if no blue staining was detected in the cells (pink arrow). MSCs were categorized low positive for SA-β-gal staining if cells show partial cytoplasmic staining (green arrow). MSCs were categorized as high positive for SA-β-gal staining if cells showed complete cytoplasmic staining (blue arrow). (B) SA-β-gal quantification of MSCs transduced with an empty overexpression lentiviral construct (Empty) or a TWIST1 overexpression lentiviral construct (TWIST1) after 11 days of expansion. N=4, 2 donors with 2 replicates per donor. (C-E) SA-β-gal quantification of MSCs treated for 24 h (C), 2 passages (D) or 4 passages (E) with scramble siRNA (Scramble) or siRNA against TWIST1 (siTWIST1). N=4-6, 2-3 donors with 2 replicates per donor. (B-E) Graphs show individual data points and grand mean of percentage of SA-β-gal negative (left), low positive (middle panel) and high positive (right panel) cells.

bioRxiv preprint doi: https://doi.org/10.1101/2020.10.11.335448; this version posted October 11, 2020. The copyright holder for this preprint (which was not certified by peer review) is the author/funder. All rights reserved. No reuse allowed without permission.

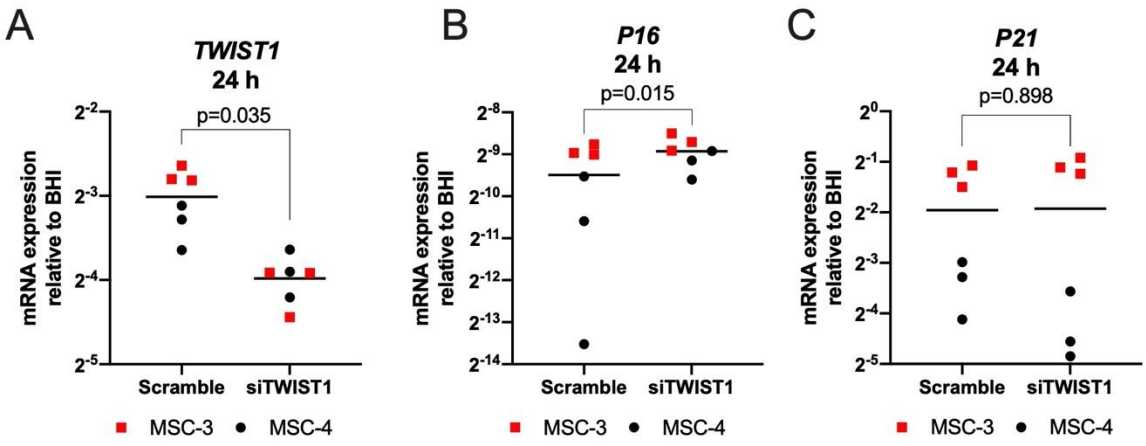

Fig EV3. Related to Fig 2. Senescence markers after 24 h and 2 passages of *TWIST1* silencing in MSCs. (A-C) *TWIST1* (A), *P16* (B), and *P21* (C) mRNA levels in MSCs treated for 24 h with scramble siRNA (Scramble) or siRNA against TWIST1 (siTWIST1). N=6-9, 2-3 donors with 3 replicates per donor, linear mixed model. Graphs show individual data points and grand mean.

bioRxiv preprint doi: https://doi.org/10.1101/2020.10.11.335448; this version posted October 11, 2020. The copyright holder for this preprint (which was not certified by peer review) is the author/funder. All rights reserved. No reuse allowed without permission.

A

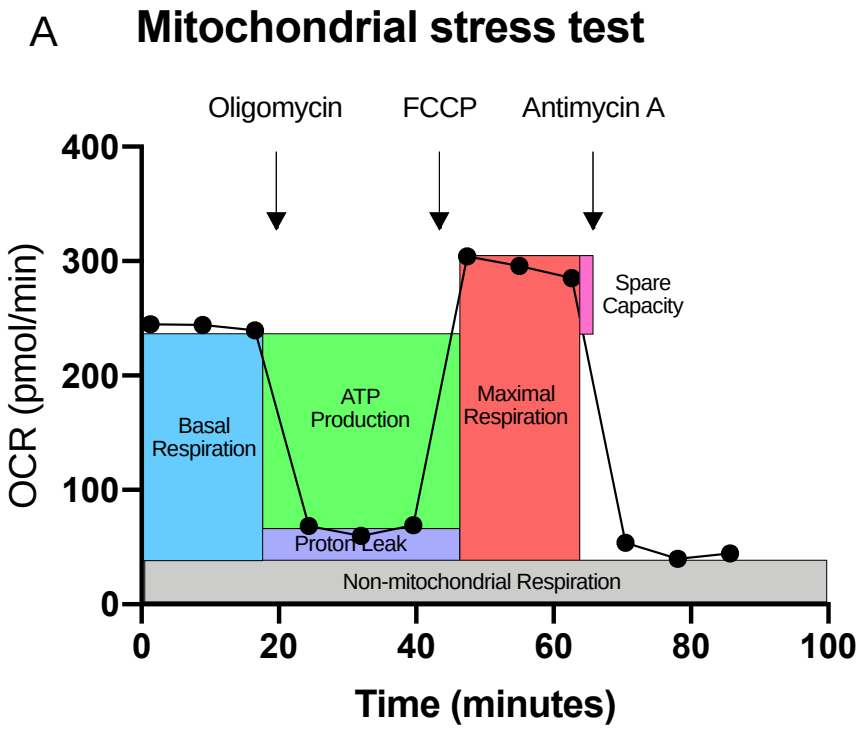

B

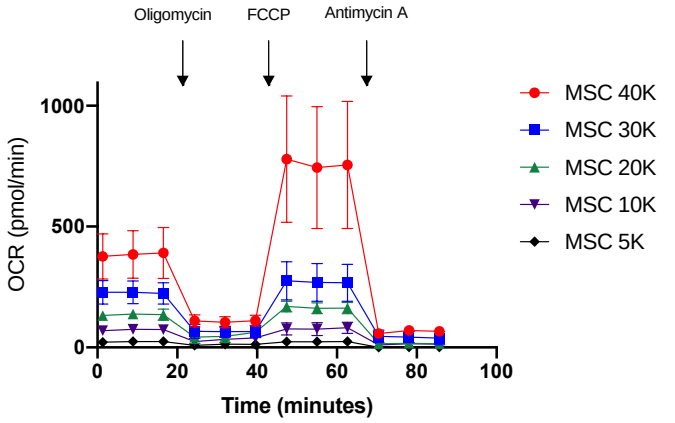

C

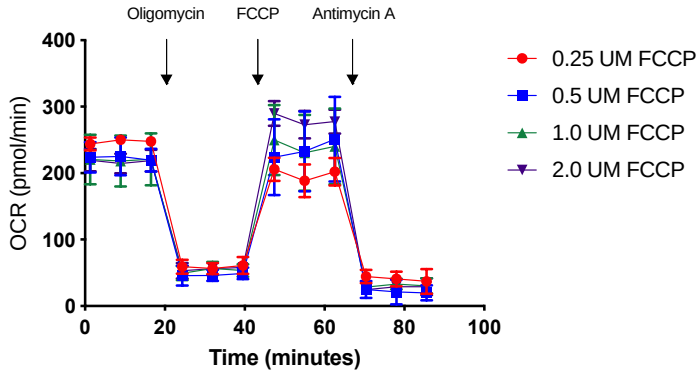

bioRxiv preprint doi: https://doi.org/10.1101/2020.10.11.335448; this version posted October 11, 2020. The copyright holder for this preprint (which was not certified by peer review) is the author/funder. All rights reserved. No reuse allowed without permission.

Fig EV4.Related to Fig3. Optimization of the cell number and FCCP concentration for the mitochondrial stress test using Seahorse technology. (A) The oxygen consumption rate (OCR) in MSCs was measured using Seahorse technology followed by subsequent measurements after injection of mitochondrial toxins: oligomycin, FCCP, and antimycin A. Using the mitochondrial stress test Basal OCR, ATP production, Maximum OCR, Spare capacity, Nonmitochondrial respiration and Proton leak were determined. (B) Mitochondrial stress test with different MSCs densities per well (5K, 10K, 20K, 30K and 40K) using 1.0 μM FCCP. (C) Mitochondrial stress test with 30K MSCs per well using different concentrations FCCP (0.25, 0.5, 1.0 and 2.0 μM). N=5-7, 1 donor with 5-7 replicates per donor. Graphs represent mean with SD.

bioRxiv preprint doi: https://doi.org/10.1101/2020.10.11.335448; this version posted October 11, 2020. The copyright holder for this preprint (which was not certified by peer review) is the author/funder. All rights reserved. No reuse allowed without permission.

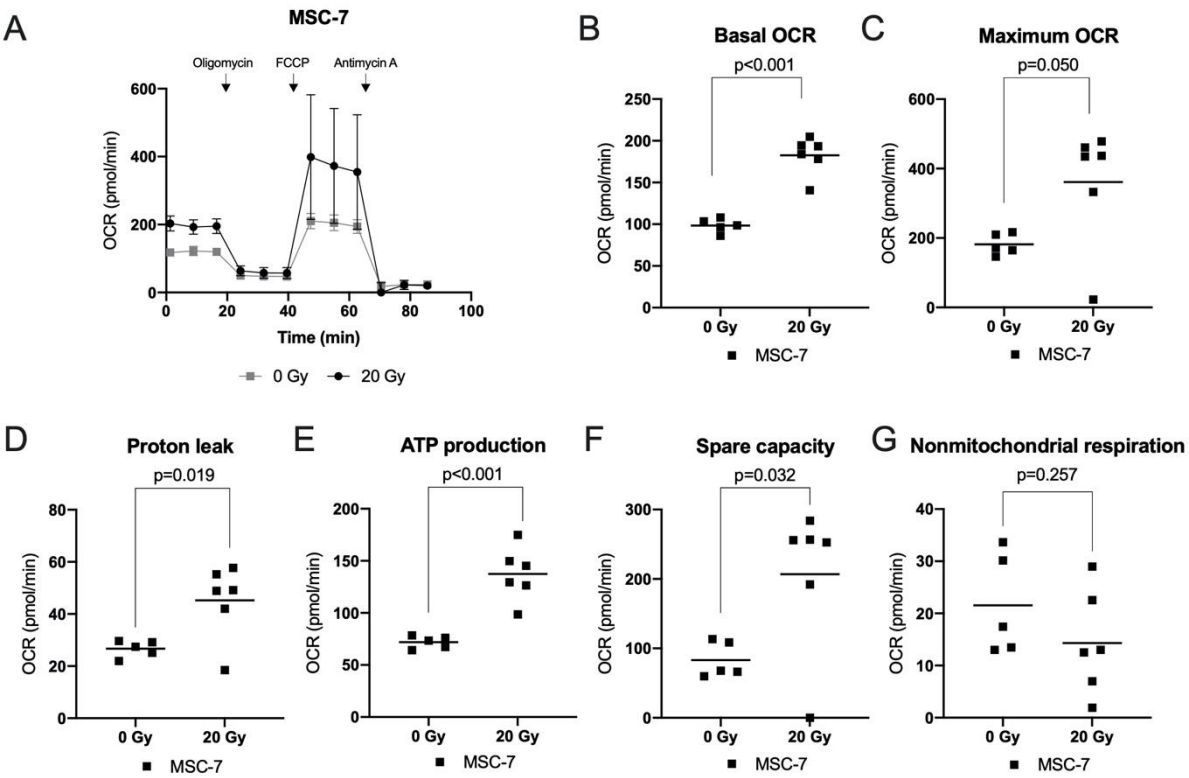

Fig EV5.Related to Fig3. Increased oxygen consumption rate (OCR) in TWIST1 silenced MSCs. (A) Graph shows the OCR in MSCs irradiated with 0 or 20 Gy after addition of oligomycin, FCCP and antimycin A. Values represent mean with SD, N=5-6 replicates. (B-G) Graphs show calculated values for basal OCR (B), maximum OCR (C), proton leak (D), ATP production (E), spare capacity (F) and non-mitochondrial respiration (G) in MSCs irradiated with 0 or 20 Gy. N=5-6 replicates, unpaired t-test. Graphs show individual data points and mean.

bioRxiv preprint doi: https://doi.org/10.1101/2020.10.11.335448; this version posted October 11, 2020. The copyright holder for this preprint (which was not certified by peer review) is the author/funder. All rights reserved. No reuse allowed without permission.

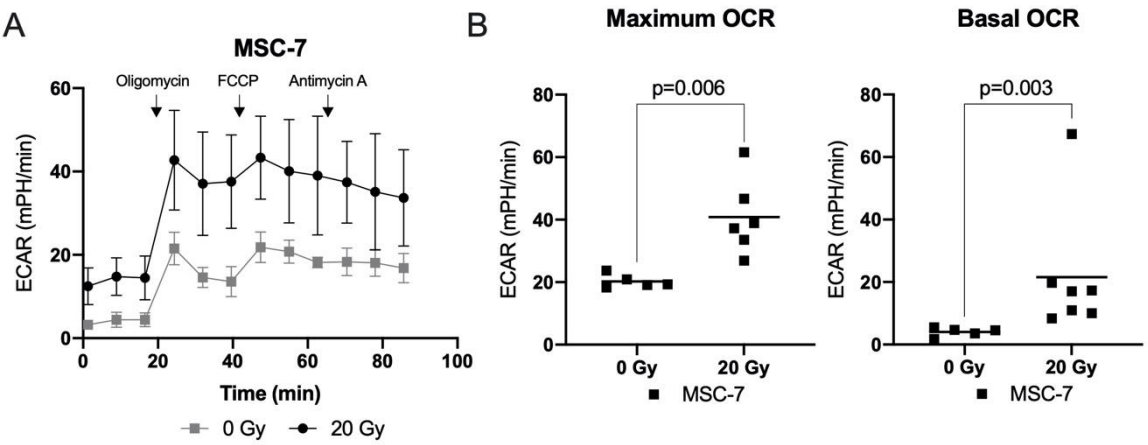

Fig EV6.Related to Fig4. Increased extrcellular acidification rate (ECAR) in irradiated MSCs.

(A) Graph shows the ECAR in MSCs irradiated with 0 or 20 Gy after addition of oligomycin, FCCP and antimycin A. Values represent mean with SD, N=5-6 replicates. (B) Graphs show ECAR values for basal OCR and maximum OCR in MSCs irradiated with 0 or 20 Gy. N=5-6 replicates, unpaired t-test. Graphs show individual data points and mean

bioRxiv preprint doi: https://doi.org/10.1101/2020.10.11.335448; this version posted October 11, 2020. The copyright holder for this preprint (which was not certified by peer review) is the author/funder. All rights reserved. No reuse allowed without permission.

Table EV1. Primer sequences

Gene	Forward	Reverse	Type of chemistry
TWIST1	5'-GTCCGCAGTCTTACGAGGAG-3'	5'-CCAGCTTGAGGGTCTGAATC-3'	SYBR Green
GAPDH	5'-ATGGGGAAGGTGAAGGTC G-3'	5'-TAAAAGCAGCCCTGGTGACC-3'	TaqMan
HPRT1	5'-TTATGGACAGGACTGAACGTCTTG-3'	5'-GCACACAGAGGGCTACCATGTG-3'	TaqMan
RPS27A	5'-TGGCTGTCCTGAAATATTATAAGGT-3'	5'-CCCCAGCACCACATTCATCA-3'	SYBR Green
IL6	5'-ACTCACCTCTTCAGAACGAATTG-3'	5'-CCATCTTTGGAAGGTTCAGGTTG-3'	SYBR Green
IL8	5'- TTTTTGAAGAGGGCTGAGAATTC-3'	5'-ATGAAGTGTTGAAGTAGATTTGCTTG-3'	SYBR Green
P21	5'-TGTCCGTCAGGACCCATGC-3'	5'-AAAGTCGAAGTTCCATCGCTC-3'	SYBR Green
P16	5'-ACCTGAGATGAGACAGGAGTC-3'	5'-ATGGAGCCTTCGGCTACT-3'	SYBR Green
CCL2	5'-GAGCCAGATGCAATCAATGCC-3'	5'-GGAATCCTGAACCCACTTCT-3'	SYBR Green
IL1B	5'-CCCTAAACAGATGAAGTGCTCCTT-3'	5'-GTAGTCGGATGCCGCCAT-3'	SYBR Green
VEGFA	5'-CTTGCCTTGCTGCTCTACC-3'	5'-CACACAGGATGGCTTGAAG-3'	SYBR Green
MMP13	5'-AAGGAGCATGGCGACTTCT-3'	5'-TGGCCCAGGAGGAAAAGC-3'	TaqMan
IL10	5'-CCTGGAGGAGGTGATGCCCCA-3'	5'-GACAGCGCCGTAGCCTCAGC-3'	SYBR Green